Earth's Future

RESEARCH ARTICLE
10.1029/2024EF005208

Current Interventions Are Inadequate to Maintain Cities' Resilience During Concurrent Drought and Excessive Heat

Yannick Back[1], Alrun Jasper-Tönnies[2], Peter M. Bach[3,4], Prashant Kumar[1], Mattheos Santamouris[5], Wolfgang Rauch[1], and Manfred Kleidorfer[1]

[1]University of Innsbruck, Unit of Environmental Engineering, Innsbruck, Austria, [2]Hydro & Meteo GmbH, Lübeck, Germany, [3]Department of Civil Engineering, Monash University, Clayton, VIC, Australia, [4]EdenCT, Dübendorf, ZH, Switzerland, [5]High Performance Architecture, School of Built Environment, University of New South Wales, Sydney, NSW, Australia

Key Points:

- Degree of surface sealing <11% and unrestricted water supply required to maintain a prevailing evaporative cooling effect over an area
- Water-limiting conditions impair evaporative capacity of urban green spaces, amplifying heat stress during extreme events
- Urgency for combined rain and greywater recycling for green space irrigation to increase cities' resilience and save water resources

Correspondence to:

Y. Back,
yannick.back@uibk.ac.at

Citation:

Back, Y., Jasper-Tönnies, A., Bach, P. M., Kumar, P., Santamouris, M., Rauch, W., & Kleidorfer, M. (2025). Current interventions are inadequate to maintain cities' resilience during concurrent drought and excessive heat. *Earth's Future*, *13*, e2024EF005208. https://doi.org/10.1029/2024EF005208

Received 7 AUG 2024
Accepted 12 FEB 2025

Author Contributions:

Conceptualization: Yannick Back
Data curation: Yannick Back
Formal analysis: Yannick Back
Funding acquisition: Manfred Kleidorfer
Investigation: Yannick Back
Methodology: Yannick Back, Alrun Jasper-Tönnies
Project administration: Manfred Kleidorfer
Resources: Yannick Back, Wolfgang Rauch, Manfred Kleidorfer
Software: Yannick Back, Alrun Jasper-Tönnies, Prashant Kumar
Supervision: Peter M. Bach, Wolfgang Rauch, Manfred Kleidorfer
Visualization: Yannick Back, Alrun Jasper-Tönnies
Writing – original draft: Yannick Back, Alrun Jasper-Tönnies

Abstract Climate change is expected to intensify the global water cycle, affecting land-atmosphere feedbacks and surface water availability. This leads to prolonged droughts and excessive heat events, increasing vulnerability of cities to water scarcity and extreme heat. Here, we integrate data from regional climate simulations into an urban modeling approach that operates at an intraurban microscale. Using this approach, we investigate the concurrent effects of the 2019 European summer drought and an increase in extreme heat days under RCP2.6 (mitigation scenario) and RCP8.5 (business-as-usual scenario) on land-atmosphere interactions, evaporative cooling potential, and bioclimatic conditions in Innsbruck, Austria. Results indicate that water-limiting conditions such as those from summer 2019 impair evaporative capacities of ecological systems and augment diurnal and nocturnal heat transfer between the soil, surface and atmosphere in the city, if not irrigated extensively. Combined with the projected increase in daily maximum temperature of extreme heat days by 3.9 K under RCP8.5, we see the development of extreme human heat stress, with a mean Universal Thermal Climate Index (UTCI) exceeding 38°C across the study area. Additionally, we found that maintaining a prevailing evaporative cooling effect over an area requires a degree of surface sealing less than 11% and unrestricted water supply. We stress the urgency of integrated urban water management, including combined rain and greywater recycling, and innovative natural and technical climate change interventions for urban green space irrigation. These mitigation measures are necessary to avoid critical malfunctions in ecological systems related to human well-being under future climate trajectories.

Plain Language Summary The frequency and simultaneous occurrence of climate extremes, such as droughts and extreme heat events, are increasing with climate change. To better understand their effects on green infrastructure, water availability, urban overheating, and human heat stress, we used information on future climate trends from regional climate simulations in a spatial modeling approach that operates at the inner city scale. As a case study, we analyze the effects of the 2019 European summer drought on the alpine city of Innsbruck, Austria. Using temperature information from regional climate models, we simulate a similar drought event with increased temperatures under climate change conditions. Our results show that unless irrigated extensively, the cooling effect generated by green spaces in the city diminishes due to drier conditions, which, in turn, increases the pressure on local and regional water resources. This means that current adaptation measures, such as nature-inspired Blue-Green Infrastructures, will not cope with longer-lasting dry periods due to a lack of sufficient and sustainable water availability. Our findings support a greater need for comprehensive urban water management, including recycled and reclaimed water from wastewater treatment plants, to irrigate green spaces in cities.

1. Introduction

The global water cycle is expected to intensify due to global warming (HELD & SODEN, 2006; HUNTINGTON, 2006), redistributing atmospheric water supply and surface water demand by means of precipitation (Pendergrass and Hartmann, 2014) and potential evapotranspiration (Scheff and Frierson, 2014) respectively. With every 1 K increase in global temperature, the water-holding capacity of the atmosphere increases by approximately 7% following the Clausius-Clapeyron equation (O'Gorman and Muller, 2010). This affects surface water availability and land-atmosphere feedbacks (Dirmeyer et al., 2012; Gerken et al., 2019).

Writing – review & editing: Yannick Back, Alrun Jasper-Tönnies, Peter M. Bach, Prashant Kumar, Wolfgang Rauch, Manfred Kleidorfer

Land-atmosphere interactions play a crucial role in the climate system (Santanello et al., 2018; Seneviratne et al., 2006), shaping atmospheric water and energy cycles (Jach et al., 2022) and, by enhancing land-atmosphere feedbacks (Dirmeyer et al., 2012), influencing the climate response to land cover change (Hirsch et al., 2014). An increase in global land evapotranspiration (Wang et al., 2022), caused by increasing temperatures and an amplification of aridity over land (Berg et al., 2016) intensified by land-atmosphere feedbacks, is already observable. Earlier spring greening in the Northern Hemisphere (driven by higher temperatures) exacerbated summer soil drying in certain regions (Lian et al., 2020). These effects can intensify climate extremes such as heatwaves and droughts (Anderegg et al., 2019; Baldwin et al., 2019; Jaeger and Seneviratne, 2011; Schumacher et al., 2022; Sousa et al., 2020), with regional hotspots identified (Cook et al., 2020) and an increase in concurrent droughts and heatwaves (Mazdiyasni and AghaKouchak, 2015).

Maintaining livability and sustainability in cities worldwide is becoming increasingly challenging as climate change alters local temperature and precipitation patterns (Bastin et al., 2019; Zhao et al., 2021), increases the occurrence of dry periods (Büntgen et al., 2021) as well as frequency of excessive heat events, extreme precipitation events, and tropical nights per year (Fischer et al., 2021). Global warming, in combination with urbanization-driven surface sealing, exposes cities worldwide to increased flash flood risk from extreme precipitation events (Arnbjerg-Nielsen et al., 2013; Doan et al., 2022) and urban overheating (Nazarian et al., 2022). Recent scientific approaches and policy interventions have addressed these aggravations at different scales and with diverse objectives by improving infiltration, evapotranspiration, and water storage capabilities, partly mimicking natural processes using engineered systems. Over time, a range of terms have emerged that describe adaptation interventions depending on the location of their origin and primary focus (Ruangpan et al., 2020). These include but are not limited to Nature-Based Solutions (Nesshöver et al., 2017), integrated stormwater management (Chocat et al., 2001), Green Infrastructure (Matsler et al., 2021) and the Sponge City concept (Nguyen et al., 2019). However, they are closely associated and provide a similar range of ecosystem services (Lafortezza et al., 2018; Maes et al., 2021; Parkinson, 2021), including enhanced local cooling and outdoor human thermal comfort (Lai et al., 2019).

Although increasing latent heat fluxes favor surface cooling, land-atmosphere feedbacks will decrease surface water availability as evapotranspiration increases (Berg et al., 2016; Lian et al., 2020; Mastrotheodoros et al., 2020; Zhou et al., 2019) due to an acceleration in the transfer of water to the atmosphere. Modelling urban climate interactions and, more specifically, climate change impacts on ecological systems and bioclimatic conditions at the intraurban microscale is of high importance to assist urban planning in designing mitigation interventions and strategies to cope with present and future consequences posed by climate change and urbanization (Oh and Sushama, 2021; Zhao et al., 2021; Zhou et al., 2022). However, the current models and approaches have two major drawbacks.

First, the resolution of the current global-scale Earth system models is too coarse to adequately account for urban surfaces and their interactions with the atmosphere in the urban canopy layer. Climate models such as the Community Climate System Model version 4 (CCSM) (Gent et al., 2011) include the parameterization of urban areas (Oleson et al., 2008) incorporated into the Community Land Model (CLM), which, in turn, is part of the CCSM. This parameterization permits the simulation of temperature in cities on a global scale (Oleson et al., 2011) and, thus, the analysis of urban heat islands (McCarthy et al., 2010; Oleson, 2012). Regional climate models (RCM) (Jeong et al., 2016), a dynamic downscaling approach, are able to conduct simulations at a higher resolution; however, they still operate on a horizontal resolution of several kilometers. Nonetheless, study results obtained using regional climate models (Bélair et al., 2018; Daniel et al., 2019; Langendijk et al., 2019) highlight the importance of including the urban canopy scheme in climate model simulations (Oh and Sushama, 2021). Due to the complex topography and a large number of small-scale atmospheric phenomena, alpine regions pose considerable challenges to climate models. Previous studies have shown that RCMs can represent the broad characteristics of alpine climates. Despite uncertainties related to the complex alpine terrain, several studies have reported consistent mean temperature trends for the European Alps (Gobiet et al., 2014; Kotlarski et al., 2010). Studies evaluating simulations from the Coordinated Regional Downscaling Experiment (EURO-CORDEX) initiative confirmed a robust warming signal (Jacob et al., 2014; Smiatek et al., 2016). The European Alps face a projected increase in mean temperature of 2.4°C until the end of the century under the representative concentration pathway (RCP) scenario RCP4.5, and 4.6°C under the RCP8.5 scenario (Jacob et al., 2014). However, the resolution of most current RCMs (e.g., 12 km of EURO-CORDEX EUR-11) is still insufficient to resolve mesoscale systems, valley flows, and spatial temperature patterns in mountainous areas (Vautard et al., 2013).

This leads to uncertainties in regional climate projections, adding to other sources of uncertainty such as future greenhouse gas emissions (Gobiet et al., 2014).

Second, spatiotemporal variability in surface water availability and its impact on promoted climate change interventions for heat mitigation (i.e., green infrastructure) on a citywide scale are insufficiently represented in current urban heat studies (Li et al., 2019; Manoli et al., 2019; Peng et al., 2012). Soil moisture, including soil moisture-temperature coupling and soil moisture-precipitation coupling, represents a key variable in the climate system, affecting near-surface air temperatures and precipitation patterns (Lorenz et al., 2016; Seneviratne et al., 2010). Soil moisture availability critically affects the intensity of urban heat islands (Manoli et al., 2020). The recently introduced urban ecohydrological model, Urban Tethys-Chloris (UT&C) (Meili et al., 2020), includes a fully coupled energy and water balance and can study the effects of varying urban landscapes on urban climate and hydrology in detail. Able to model time series of soil moisture and its effects on plant water stress, Meili et al. (2020) have shown in detail the relationship between dry periods, soil moisture, and latent heat fluxes and have analyzed plant performance under water-limiting conditions, changing climatic conditions, and different irrigation practices. However, the spatial variability of UT&C is limited, which does not allow the investigation of changes on a citywide scale, as simulations can only be conducted in a predefined urban canyon with a specified geometry, tree arrangement, and possible fractions of ground and roof surfaces (Zhang et al., 2022). Therefore, the impacts of increasing land aridity due to amplified land-atmosphere feedbacks on urban ecological systems and the resulting changes in meteorological conditions at the citywide scale remain elusive.

Here, we show the effects of water-limiting conditions and increasing daily maximum temperatures of extreme heat days (days exceeding the 97th percentile of Tmax) under future climate trajectories on land-atmosphere interactions, evaporative cooling potential, and bioclimatic conditions in Innsbruck, Austria, using information about future climate trends from regional climate simulations in an urban modelling approach that operates at citywide to microscale. We investigate the effects of the 2019 European summer drought (Blauhut et al., 2022; Rakovec et al., 2022), on (a) land-atmosphere interactions by means of changing surface energy flux partitioning, (b) vegetation health and evaporative cooling potential by means of vegetation water content and potential evapotranspiration, and (c) bioclimatic conditions by means of changes in the Universal Thermal Climate Index (UTCI).

2. Methodology

Land-atmosphere interactions, vegetation health, and evaporative cooling potential are calculated across the entire city, whereas UTCI is calculated within a specific case study area within the city, all with a spatial resolution of 0.2 m. In addition to the drought effects, we account for the impacts of increasing daily maximum temperature of hot heat days on bioclimatic conditions (namely the UTCI) under the representative concentration pathways (RCPs) RCP2.6 (mitigation scenario) and RCP8.5 (business-as-usual scenario). Estimations of current and future hot days are derived from regional climate simulations conducted in the EURO-CORDEX initiative (Jacob et al., 2014) and the Regional Climate change Ensemble simulations for Germany (ReKLiEs) project (Hoffmann et al., 2018). To conduct calculations on a citywide to urban microscale, we use an integrated modeling approach based on Back et al. (2023) coupling capabilities of Computational Fluid Dynamics (CFD) and Geographic Information Systems (GIS) modeling. This approach allows us to account for the complexity of the urban structure and specific surface characteristics on a fine spatial scale using GIS and to include the complexity of flow dynamics within the built environment using CFD. To assess changes in land-atmosphere interactions, we use a novel Bowen ratio-based threshold that describes the surface induced cooling and warming effect, based on the surface energy fluxes, on climatic conditions in the urban canopy layer, introduced by Back et al. (2024). The threshold separates the surface induced cooling effect (higher proportion of latent heat fluxes increasing evaporative cooling) from the warming effect (higher proportion of combined sensible and substrate heat fluxes increasing heat transfer between the surface, soil, and atmosphere), and is indicated by a Bowen ratio of 0.52. The derivation of the exact number defining the threshold is described in detail in Section 2.6. Finally, we use the existing strong linear relationship between the degree of surface sealing and the Bowen ratio to investigate the amount of greenery needed to maintain a prevailing evaporative cooling effect (Bowen ratio <0.52), assuming an unrestricted water supply. On this basis, we discuss the importance of water availability to sustain ecological systems in cities under future climate change trajectories and urge on improving cities' resilience beyond current climate change interventions to cope with future consequences, especially water scarcity.

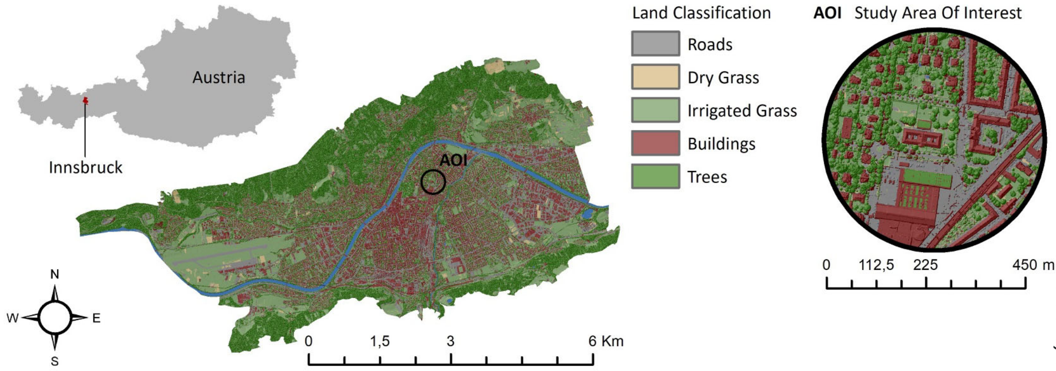

Figure 1. Case study overview showing geographic location of the city of Innsbruck in Tirol, Austria, and the land cover classification for Innsbruck as well as for the study area of interest.

2.1. Study Area

The selected case study is the Alpine city of Innsbruck, the capital of Tyrol in western Austria, situated in the Inn valley at an elevation of approximately 574 m. With a surface area of 36.6 km^2, the city comprises different structure types of varying density and height, and is populated by approximately 130,000 citizens. For detailed investigations in this study, we focus on an area located northeast of the city center of Innsbruck (Figure 1). With approximately 2,000 ha, the area comprises a variety of building heights, surface and vegetation types, and street widths. The city of Innsbruck was chosen due to the availability of detailed CIR (Colored Infrared)-imagery with a spatial resolution of 0.2 m. CIR imagery is a type of multispectral imagery that captures information in the near-infrared, red and green wavelengths of the electromagnetic spectrum. This makes them particularly useful for analyzing vegetation health, water bodies, and land cover because of their different abilities to reflect and absorb different wavelengths. CIR images form the basis for calculations in the GIS-based modeling approach. The high spatial resolution (0.2 m) of the input CIR image data determines the spatial accuracy of the output data. The area northeast of the city center of Innsbruck was chosen because of the availability of a 3D model of the urban infrastructure. This model forms the basis for calculations using the CFD software. Together, the detailed CIR imagery and comprehensive 3D model allowed us to perform our analysis with exceptionally high precision, ensuring that both spatial and structural characteristics were captured accurately in our modeling efforts.

2.2. Regional Climate Scenarios From EURO-CORDEX and ReKLiEs

Within the EURO-CORDEX initiative, regional climate projections for impact research were produced by an international framework. EURO-CORDEX is part of the global Coordinated Regional Downscaling Experiment (CORDEX, http://wcrp-cordex.ipsl.jussieu.fr/; Giorgi et al. (2009)). The regional simulations downscale CMIP5 global climate projections (Taylor et al., 2012) based on scenarios of the RCPs (Moss et al., 2010; van Vuuren et al., 2011). Simulations are provided on standardized grids with two horizontal resolutions: 0.44° (EUR-44) and 0.11° (EUR-11). In the German project ReKliEs, EURO-CORDEX simulations are complemented by dynamic and statistical simulations. These were produced using the RCP scenarios RCP2.6 ("mitigation") and RCP8.5 ("business-as-usual") and provided on the EURO-CORDEX grid EUR-11 with 0.11° horizontal resolution. The ReKliEs domain covers Germany and adjacent large river catchments draining into Germany including the region around Innsbruck. In addition, several climate indices, such as hot and summer days, are provided for impact research. Indices defined by a fixed threshold are sensitive to model-specific biases. To account for these biases, an "implicit" bias correction was conducted within ReKliEs using individually adjusted thresholds for each model (Hoffmann et al., 2018). Individual thresholds were determined by comparing the frequency of threshold exceedances between the model results and observations during the reference period. Simulations from the ReKliEs project (see Table 1) were considered for the evaluation of heat indices (see Table 1 for a list of the considered GCM/RCM combinations and contributing institutes). The analysis encompassed the periods 2021–2050 and 2071–2100 compared with the reference period 1971–2000.

10.1029/2024EF005208

Table 1
EURO-CORDEX/ReKliEs Simulations With the Combinations of Global and Regional Climate Models, the Attributing Institutes and the RCP-Scenarios (See www.euro-cordex.net and http://reklies.hlnug.de/home for Details)

RCM GCM	CLMcom-CCLM4 (CLM-Community)	DMI-HIRHAM5 (DMI)	KNMI-RACMO22 (KNMI)	SMHI-RCA4 (SMHI)
CERFACS-CNRM-CM5 (CERFACS)	*r1i1p1 RCP8.5*			*r1i1p1 RCP8.5*
ICHEC-EC-EARTH (SMHI)	*r12i1p1 RCP2.6 & RCP8.5*	*r3i1p1 RCP2.6 & RCP8.5*	*r1i1p1 RCP2.6 & RCP8.5*	*r12i1p1 RCP2.6 & RCP8.5*
MOHC-HadGEM2-ES (MOHC)			*r1i1p1 RCP2.6 & RCP8.5*	*r1i1p1 RCP2.6 & RCP8.5*
MPI-M-MPI-ESM-LR (MPI)	*r1i1p1 RCP2.6 & RCP8.5*			

Note. The notation rX iY pZ (e.g., r12i1p1) represents different simulations of a climate model, where rX is the realization (ensemble member), iY is the initialization method, and pZ is the physics version, with simulations conducted under different emission scenarios like RCP2.6 (low emissions) and RCP8.5 (high emissions).

2.3. Meteorological Measurement Data

The records of two meteorological stations in Innsbruck are used with parameters of air temperature, air pressure, wind speed, and cloud cover (provided by Geosphere Austria in Innsbruck). The quality controlled observations from the stations *Innsbruck Airport* and *Innsbruck University* spanned a period from 1952 to 2009.

2.4. Extreme Heat Indices From RCM and Observations

Trends in mean air temperatures and heat indices were analyzed as a basis for the impact assessment of future heat events. We use two indices for extreme heat: (a) the number of "hot days", defined as the number of days per year with a daily maximum temperature (T_{max}) above the fixed threshold 30°C—a temperature above which the human body starts to suffer from increased heat stress (Asseng et al., 2021)—and (b) the 97th percentile of Tmax (Tmax_Q97). Days with Tmax exceeding Tmax_Q97 are referred to as "extreme heat days." Climate change signals were computed from the regional climate projections listed in Table 1 as statistical mean changes averaged over six model grid points around Innsbruck. This area comprises not only the Inn valley but also parts of the surrounding mountains with an average elevation above Innsbruck city situated at 574 m. The elevation differences affect the mean and extreme temperatures, as well as the model-derived number of "hot days." To derive the non-biased trends of hot days at the Innsbruck station level, several steps were carried out. First, the climate change signals of the number of hot days were computed as 30-year averages of the periods 2021–2050 and 2071–2100 in relation to the reference period 1971–2000. Second, the exceedance probability of the 30°C threshold was related to the observed Tmax at station level ($Tmax_{obs}$), using histogram data of $Tmax_{obs}$ at the stations *Innsbruck Airport* and *Innsbruck University* from 1971 to 2000 (see Figure 2). At these stations, the 30°C threshold was exceeded an average approximately 10 days per year, corresponding to Tmax_Q97 over the observation period. We estimated Tmax_Q97 for future periods ($Tmax\_Q97_f$) under the assumption that the shape of the extreme tail

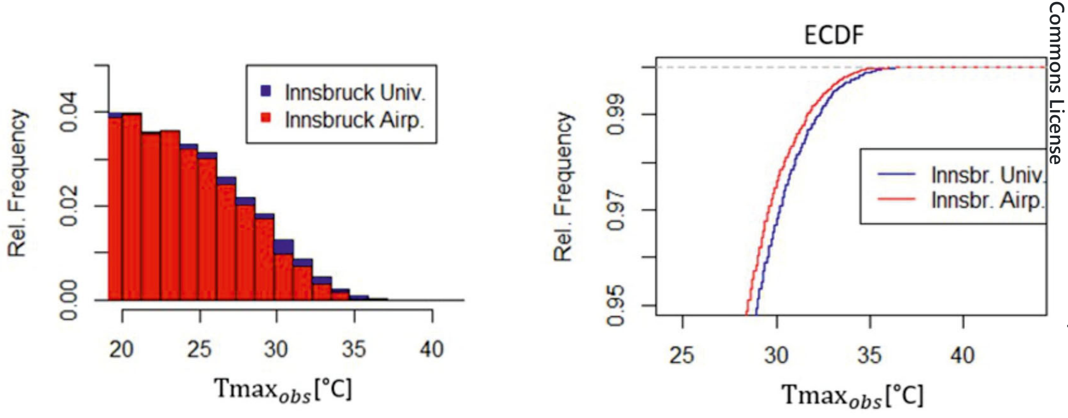

Figure 2. Histogram (left) and Empirical Cumulative Distribution Function (ECDF) of $Tmax_{obs}$ at the ZAMG meteorological stations *Innsbruck University* and *Innsbruck Airport* in the period 1971–2000. Sections show $Tmax_{obs}$ above 20°C in the histogram and the highest 5% of $Tmax_{obs}$ in the ECDF.

of the probability distribution function (PDF) of Tmax will not change in comparison to the observed PDF. Days with maximum air temperatures reaching Tmax_Q97 and Tmax_$Q97_f$ were selected from the observation data set as representatives for reference and future extreme heat days.

2.5. CFD-GIS Integrated Modeling Approach

To perform fine-scale simulations for land surface temperature (LST), mean radiant temperature (MRT) and Universal Thermal Climate Index (UTCI) in a 2D urban environment, we used a geographic information system (GIS)-based modeling approach, which was introduced by Back et al. (2021). The proposed modeling approach combines a fine-scale surface classification comprising eight different surface classes, thermal characteristics (global radiation, direct radiation, and diffuse radiation), surface characteristics (emissivity and Bowen ratio values), and meteorological input data. Based on this combined data set and well-established physical relations in the model setup, our model uses an adapted approach from Matzarakis et al. (2010) and Bröde et al. (2010) to first evaluate LST, followed by MRT and finally UTCI.

To enable comprehensive analysis of fine-scale land-atmosphere interactions and their effects on the urban climate system, Back et al. (2023) extended this modeling approach by combining the GIS-based approach with the capabilities of computational fluid dynamics (CFD) software. This integrates the CFD-generated horizontal and vertical variabilities in wind speed and air temperature patterns within the urban canopy layer into the existing GIS-based approach. Specifically, we used a height of 1.75 m to model bioclimatic conditions (MRT and UTCI), whereas a height of 0.2 m was used to calculate LST. Furthermore, based on Back et al. (2024), we calculated the quantitative values of all three fluxes of the surface energy balance (latent heat flux (LE), sensible heat flux (H), and substrate heat flux (G)), net all-wave radiation (Q), the vegetation water content (VWC), and potential evapotranspiration (PET) at a very fine scale (0.2 m). In this study, we used CIR imagery to calculate the Normalized Difference Vegetation Index (NDVI), which, in turn, enables us to determine VWC, PET, Bowen ratio, net-all wave radiation (Q), and surface energy fluxes (LE, H and G) using specific NDVI-based equations that were described in detail by Back et al. (2024) in the Supporting Information appendix as Equations S1, S2, S3, S11–S20, and S21 in the order of the above variables. Supporting Information can be downloaded directly from the online version of the published paper (https://agupubs.onlinelibrary.wiley.com/doi/10.1029/2023JD039723). Due to length constraints, we are unable to include all equations in this paper; however, we present the calculations for VWC, PET, the Bowen Ratio, and UTCI using Equations 1–6, as they are essential to this study.

The local government of Tyrol *Land Tirol* provided CIR Imagery captured in late August 2016 and 2019. Both years indicate different preconditions in terms of water availability detectable in the CIR images and NDVI data sets. The CIR image captured in late August 2016 represents wet preconditions, with the recorded accumulated daily precipitation for the summer months (490 mm) June, July, and August well above the long-term average of accumulated daily summer precipitation between 1961 and 1990 (358 mm). The CIR image captured in late August 2019 represents dry preconditions, with a recorded accumulated daily precipitation of 269 mm for the summer months. The 2019 image represents the summer drought (Rakovec et al., 2022) and heatwave (Sousa et al., 2020; Xu et al., 2020) that prevailed across the European continent. Recorded accumulated daily precipitation valus were obtained from the online climate monitoring service provided by Geosphere Austria (2024).

We used the NDVI derived from CIR imagery to determine the vegetation water content, Bowen ratio, net all-wave radiation, and surface energy fluxes (latent heat, sensible heat, and substrate heat fluxes). The specific NDVI-based equations are described in detail in the Supporting Information appendix of Back et al. (2024) and can be downloaded freely as mentioned above. Although NDVI acts as a determinant in the calculation of all these variables, the relationships between NDVI and each variable are derived from empirical research and physical relationships from previous studies. For the vegetation water content, we refer to Chan et al. (2013); for the Bowen ratio, we refer to Rigo (2006) and Back et al. (2023); for the net all-wave radiation and the surface energy fluxes, we refer to Kustas and Daughtry (1990), Parlow (2003), Rigo and Parlow (2007), and the calculation procedure in Back et al. (2023), as well as the Supporting Information appendix of Back et al. (2024). With the spectral information of the surfaces in absorbing and reflecting different wavelengths of the electromagnetic spectrum embedded in the CIR-based NDVI, the latter provides vital information about the interactions of different surface properties with both the underlying soil and overlying atmosphere. Therefore, integrating NDVI in the calculations supports a more detailed, holistic approach to modelling land-atmosphere interactions at fine scales.

2.5.1. Vegetation Water Content

We calculated the vegetation water content (VWC) [kg/m^2] using Equation 1, which is based on the approach of Chan et al. (2013), comprising two terms: (a) foliage water content and (b) stem water content, using NDVI and a stem factor to estimate VWC.

$$\mathrm{VWC} = 1.9134 * \mathrm{NDVI}^2 - 0.3215 * \mathrm{NDVI} + \text{stem factor} \cdot \frac{\mathrm{NDVI}_{max} - \mathrm{NDVI}_{min}}{1 - \mathrm{NDVI}_{min}}. \quad (1)$$

Based on the vegetation types in our case study area, we distinguished between grassland and trees (mixed forest) using stem factors of 1.50 and 12.77, respectively.

2.5.2. Potential Evapotranspiration

We calculated potential evapotranspiration (PET) [mm/h] using an approach introduced by Back et al. (2024), based on Lang et al. (2017) and McMahon et al. (2013) and on a proposed simplified version to determine PET from Priestley and Taylor (1972) using Equation 2:

$$\mathrm{PET} = \alpha \cdot \frac{\Delta}{\Delta + \gamma} \cdot \frac{\mathrm{Q} - \mathrm{G}}{\lambda}, \quad (2)$$

where Δ represents the slope of the saturation vapor pressure function [kPa/°C], γ is the psychrometric constant [kPa/°C], Q is the net all-wave radiation [W/m^2], G is the substrate heat flux [W/m^2], and λ is the latent heat of vapourization [MJ/kg]. Based on Priestley and Taylor (1972) and Lang et al. (2017), α represents unity for saturated surfaces and was estimated using Equation 3:

$$\alpha = \frac{\mathrm{LE}}{\frac{\Delta}{\Delta + \gamma} * \mathrm{AE}}, \quad (3)$$

where LE is the latent heat flux, and AE is the available energy (Q-G). As α strongly correlates with the Bowen ratio (Priestley and Taylor, 1972), we used Equation 3 to estimate α for different land surface covers associated with varying Bowen ratios.

As mentioned above, the underlying data set for the calculations in the GIS modeling approach is CIR imagery, a type of multispectral imagery that captures information in the near-infrared, red, and green wavelengths of the electromagnetic spectrum. The CIR image provides valuable insights into the surface properties and their interactions with both the underlying soil and the overlying atmosphere by capturing variations in reflectance and absorption at different wavelengths of the electromagnetic spectrum. This spectral information, which reveals how different materials absorb or reflect infrared light, is also embedded in the NDVI, which is calculated directly from the CIR image. One of the limitations of existing PET equations is their inability to account for changes in net all-wave radiation under varying moisture conditions, both dry and wet (Zhou and Yu, 2024). By incorporating NDVI along with meteorological variables, we are able to incorporate detailed information about soil and surface characteristics into our PET calculation. This approach allows for a more accurate representation of surface properties and soil-surface-atmosphere interactions under varying conditions, in particular through the surface reflectance properties and the associated repartitioning of the energy into the three surface energy fluxes (LE, H, and G), as described in our previous study (Back et al., 2024). This allowed us to better account for small scale variations in net all-wave radiation in the calculations for PET.

2.5.3. Bowen Ratio

The Bowen ratio (β) was derived based on the NDVI approach presented in (Back et al., 2023) as follows:

$$\beta = 1.534 \cdot \mathrm{e}^{-3.205 \cdot \mathrm{NDVI}}. \quad (4)$$

2.5.4. Universal Thermal Climate Index

Preliminary to the UTCI calculations, we calculated the MRT based on Back et al. (2021) using Equation 5:

$$\mathrm{MRT} = \left(\frac{1}{\sigma}\cdot\left(\left(\mathrm{E} + \mathrm{a_k}\cdot\frac{\mathrm{D_s}}{\varepsilon_\mathrm{p}}\right)\cdot\left(1-\frac{\mathrm{SVF}}{2}\right) + \left(\mathrm{A} + \mathrm{a_k}\cdot\frac{\mathrm{D_d}}{\varepsilon_\mathrm{p}}\right)\cdot\frac{\mathrm{SVF}}{2}\right) + \frac{\mathrm{f_p}\cdot\mathrm{a_k}\cdot\mathrm{I}^*}{\varepsilon_\mathrm{p}\cdot\sigma}\right)^{0{,}25}, \tag{5}$$

Where E [W/m^2] is the long-wave radiation flux density emitted by the surface, A [W/m^2] is the atmospheric radiation, SVF is the Sky View Factor, I* is the radiation intensity of the sun on a surface perpendicular to the incident radiation direction, a_k is the absorption coefficient of the irradiated body surface area of short-wave radiation (standard value for the human body of 0.7), ε_p is the emission coefficient of the human body (standard value of 0.97) and f_P is the surface projection factor. Using this, we calculated UTCI using Equation 6:

$$\mathrm{UTCI} = T_\mathrm{a} + \mathrm{Offset}(T_\mathrm{a}, \mathrm{MRT} - T_\mathrm{a}, U_\mathrm{Wind}, P_\mathrm{Vapour}), \tag{6}$$

where T_a is the air temperature [°C], U_{Wind} is the wind speed [m/s], and P_{Vapour} is the water vapor pressure [kPa].

2.6. Surface Induced Cooling and Warming Effect

We previously demonstrated the relationship between the surface energy fluxes, PET, VWC, UTCI, Bowen ratio, NDVI, and varying meteorological conditions under buoyancy-driven atmospheric conditions using fine-resolution results from the integrated CFD-GIS modeling approach described above (Back et al., 2024). This study introduced a Bowen ratio-based threshold to separate the surface induced cooling effect (higher proportion of latent heat fluxes increasing evaporative cooling) from the warming effect (higher proportion of combined sensible and substrate heat fluxes increasing the heat transfer between the surface, soil, and atmosphere). Back et al. (2024) found this threshold at a Bowen ratio of 0.52, matching the NDVI value of 0.33. Here, we used this threshold to describe the drought effects on land-atmosphere interactions (comparing the data sets from 2016 to those from 2019) and to determine the amount of greenery necessary to maintain a prevailing evaporative cooling effect (staying below a Bowen ratio of 0.52), assuming an unrestricted water supply, by analyzing the linear relationship between the degree of surface sealing and the Bowen ratio. It should be noted that the use of NDVI to calculate the threshold based on the Bowen ratio has a drawback in that it is unable to distinguish between wet and dry bare ground, and that it is currently only designed for land areas and therefore cannot calculate water areas, including rivers, lakes, and ponds of detectable size. As a result, this study focuses only on land areas, neglecting urban water bodies, and focusing only on evaporative cooling from vegetated areas.

3. Results and Discussion

3.1. Overall Shifts in Daily Maximum Temperature

The simulated occurrence and intensity of rising temperatures and frequencies of future extreme heat events depend on the location and the considered scenario. The ensemble of regional climate simulations from EURO-CORDEX/ReKlies in Table 1 was analyzed. Looking at the number of hot days with Tmax exceeding 30°C reveals a relatively small increase and little scenario differences until 2050 and a strong increase in RCP8.5 based simulations toward the end of the century (Figure 3). From 2050 onwards, the spread among scenarios begins to diverge significantly compared with the spread between individual models.

The change in $\mathrm{Tmax\_Q97_f}$ displays the same overall picture as the change in the number of hot days (Figure 3). Until the end of the century, $\mathrm{Tmax\_Q97_f}$ is projected to increase by 1.0 K in RCP2.6 simulations and by 3.9 K in RCP8.5 simulations. For the period 2021–2050, the scenario difference is almost negligible. For the period 2071–2100 under the scenario RCP8.5, $\mathrm{Tmax\_Q97_f}$ is likely to rise by +3.4 to +5.1 K (15%–85% percentiles) with a median of +3.9 K. Under the RCP2.6 scenario, the projected range is +0.5 to +1.4 K (median: +1.0 K). The median of $\mathrm{Tmax\_Q97_f}$ reaches 31°C for the near and the far future under the scenario RCP2.6, and 31°C and 33.9°C respectively, for 2035 and 2085 under the scenario RCP8.5. Regarding the number of hot days at the station level using the Empirical Cumulative Distribution Function (ECDF) data shown in Figure 2, this corresponds to an increase in the exceedance frequency of +20% to +70% under the RCP2.6 scenario and to an increase of a factor of three to five under the RCP8.5 scenario, compared to the reference period.

10.1029/2024EF005208

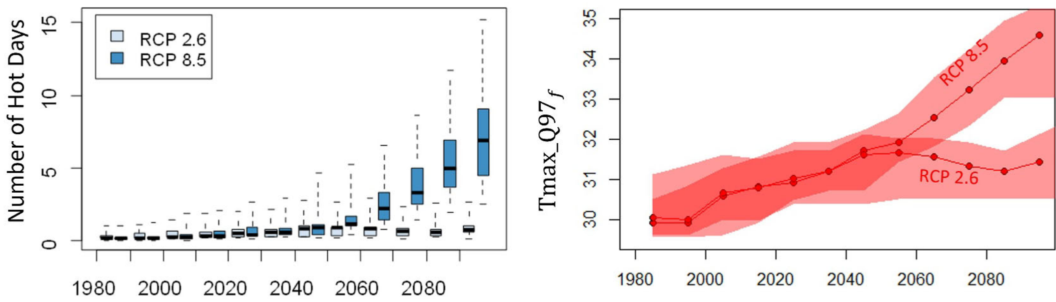

Figure 3. Left: Average number of Hot Days (daily maximum air temperature ≥30°C) per year in EURO-CORDEX/ReKliEs projections with the scenarios RCP2.6 and RCP8.5. Boxplots illustrate the ensemble spread, whiskers extend to the minimum and maximum of the simulations. Values are averaged over 30 years and 6 RCM grid points around Innsbruck, Tyrol. Right: Projected change of the 97% quantile of daily maximum temperatures $Tmax_{\_Q97}$ at Innsbruck stations, based on RCP2.6 and RCP8.5 simulations. The shaded area comprises 85% of the RCP2.6 and RCP8.5 simulations.

3.2. Drought Alters Land-Atmosphere Interactions

During the 2019 Central European drought, the Bowen ratio increased on all surfaces across Innsbruck, except for irrigated agricultural land. With sufficient available water, only these surfaces show negative changes in the Bowen ratio (Figure 4). The highest change in Bowen ratio can be found within the city (Figure 4c), while the lowest (except for agricultural land) can be found in the surrounding forests (Figure 4a). The proportion of areas with Bowen ratios below 0.52 (i.e., surface induced cooling effect (CE) exceeds warming effect (WE)) decreased from 49.3% in 2016 to 16.9% in 2019 (Figure 4b). With a shift to higher Bowen ratios, less energy is repartitioned into the latent heat flux and more into the sensible and substrate heat fluxes. This consequently enhances the warming effect within the urban canopy layer as less energy is available for evaporative cooling. Consequently, increases in sensible and substrate heat fluxes lead to higher diurnal and nocturnal air temperatures. Based on the Bowen ratio threshold named above, most vegetated surfaces have moved from a wet soil moisture regime and an energy limited evaporative-driven cooling effect (Bowen ratio between 0 and 0.52) to a transitional soil moisture

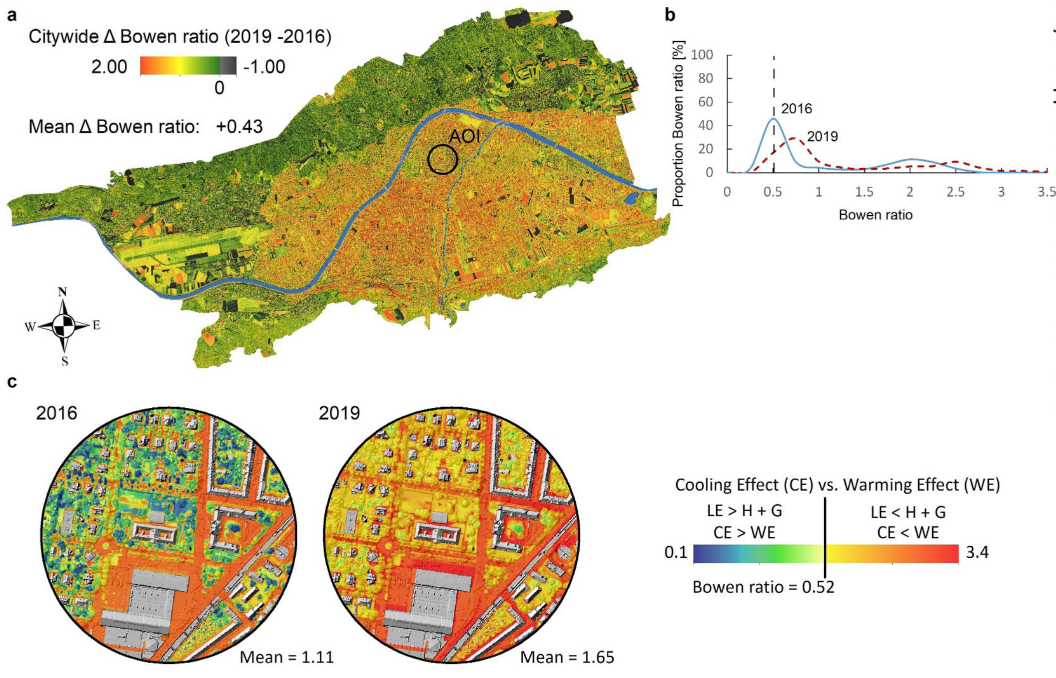

Figure 4. (a) Change in Bowen ratio between 2016 and 2019 in Innsbruck; (b) Change in proportion of Bowen ratios for the entire city, the horizontal axis depicts the Bowen ratio, and the vertical axis depicts the proportion of Bowen ratio values across the entire city. (c) Change in the Bowen ratio-based threshold in the area of interest between 2016 and 2019.

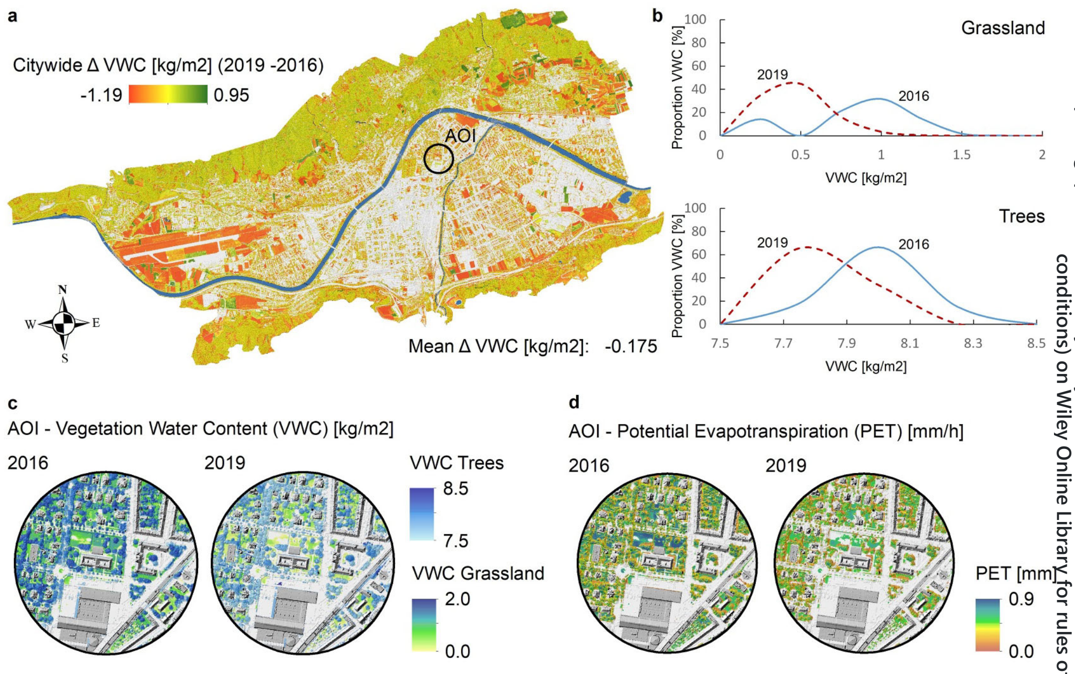

Figure 5. (a) Difference in vegetation water content (VWC) 2019 compared to 2016 in Innsbruck; (b) Proportion of VWC for grassland and trees in 2016 and 2019, the horizontal axes depict VWC, and the vertical axes depict the proportion of VWC values in areas defined as grassland and in areas defined as trees respectively across the entire city; (c) Absolute values of VWC for 2016 and for 2019; (d) Potential evapotranspiration (PET) for 2016 and for 2019.

regime and a soil moisture/water limited evaporative-driven cooling effect (Bowen ratio between 0.52 and 1.0). This means that available water for evaporation among vegetation will become the limiting factor as opposed to the amount of incoming solar radiation. An increase in substrate heat fluxes and, thus, an increase in heat transfer from the surface to the underlying soil during the day additionally leads to an increase in nocturnal intraurban heat due to enhanced heat transfer from the surface to the atmosphere as the process reverses at night. These effects are detectable in areas with a Bowen ratio above 2.0, with a higher proportion of substrate heat flux and surfaces that slowly heat up during the day and slowly cool down at night. The proportion of areas with Bowen ratios above 2.0 increased from 4.3% in 2016 to 21.8% in 2019 (Figure 4b). This is especially visible in areas of the city with a higher degree of surface sealing, such as the city center located south of the area of interest (AOI).

3.3. Drought Alters Evaporative Cooling Potential

Mean VWC decreased by -0.175 kg/m^2 (Figure 5a) in 2019 compared to 2016 across the entire city. Areas of positive change in VWC correlate with areas of negative change in Bowen ratio, highlighting sufficient water availability for well-irrigated agricultural land. The deficit in water availability across the entire city is shown to lead to a decrease in the evaporative-driven cooling effect, which is also reflected in a reduced PET (Figure 5d). Due to changing surface properties toward drier conditions (changes in the Bowen ratio and energy flux partitioning visible in Figure 4), less energy is repartitioned into latent heat, which causes the observable reduction in PET on vegetated surfaces. As mentioned in Section 2.5.2, one of the limitations of existing PET equations is their inability to account for changes in the net all-wave radiation under varying moisture conditions (Zhou and Yu, 2024). Our approach allows for a more accurate representation of surface properties and soil-surface-atmosphere interactions under varying conditions through the surface reflectance properties, captured by the CIR image, and the associated repartitioning of the energy into the three surface energy fluxes (LE, H, and G), calculated using the CIR-borne NDVI-based equations. As less energy is repartitioned into the latent heat flux, more energy is repartitioned into the sensible and substrate heat fluxes, leaving less energy potentially available for evaporative processes on vegetated surfaces. This variability in PET is visible within both the 2016 and 2019 images in Figure 5, as is the overall change in PET within the 2019 image in Figure 5. The evaporative-driven cooling effect across the city appears predominantly to be soil moisture/water limited, as most of the

10.1029/2024EF005208

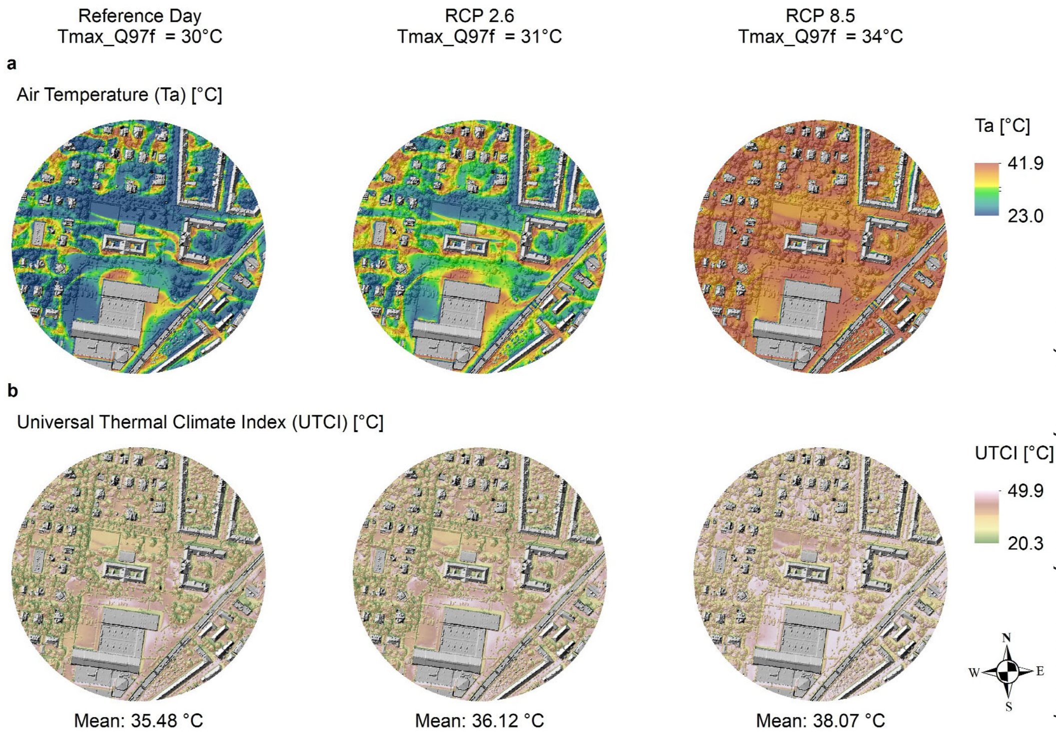

Figure 6. Comparison of 2019 modeled air temperature (top row) and Universal Thermal Climate Index (UTCI) (bottom row) for the reference day with a daily maximum air temperature of 30°C as well as for simulated future days with Tmax reaching Tmax_Q97$_f$ (Tmax = 31°C and Tmax = 34°C under RCP2.6 and RCP8.5 respectively).

vegetation shifted to a transitional soil moisture regime due to the lack of water availability. Combined with the observed reduction in VWC (Figures 5a–5c), it is evident that the evaporative capacity of vegetation across Innsbruck has become impaired by the water-limiting conditions due to the drought.

3.4. Changes in Bioclimatic Conditions in a Warmer and Dryer World

The effects on bioclimatic conditions are estimated by means of UTCI at a height of 1.75 m. Following the simulated shifts in daily maximum temperature, calculations are conducted using meteorological observation data of days where Tmax equals Tmax_Q97 for the reference period (T_{max} = 30°C), and for the far future under RCP 2.6 (T_{max} = 31°C) and RCP 8.5 (T_{max} = 34°C). Air temperature distribution across the case study using the integrated CFD-GIS modeling approach based on these initial conditions is shown in Figure 6a. Mean UTCI across the entire case study increased by 2.59°C under the business-as-usual scenario RCP8.5 (Figure 6b). While UTCI values below 32°C (corresponding to a moderate heat load) were reached during conditions of the reference day, heat stress under RCP8.5 must be classified as "very strong", with a mean UTCI throughout the case study area above 38°C. UTCI values in this range lead to extreme heat stress of humans (Tomczyk and Owczarek, 2020) and to conditions that are particularly dangerous for infants, people with a predisposed medical condition and elderly people. Especially sealed surfaces such as streets pose a significant heat stress to humans with a mean UTCI of 39.65°C under RCP8.5. Under the mitigation scenario RCP2.6, mean UTCI increased by 0.64°C. Differences in UTCI due to dryer conditions appear negligible above sealed surfaces, with a mean difference between 2016 and 2019 of 0.02°C. In contrast, grasslands show a mean difference in UTCI due to dryer conditions of 0.77°C. This exceeds differences in mean UTCI due to warmer conditions under RCP2.6 (0.71°C), compared to the reference day, by 0.06°C. This leads to the assumption that, while reaching a mitigation scenario, the effect of droughts above urban grasslands still exceeds the effects of warmer conditions on the UTCI. With a difference in mean UTCI of 2.63°C, the effects of warmer conditions exceed the effects of droughts over grassland under RCP8.5.

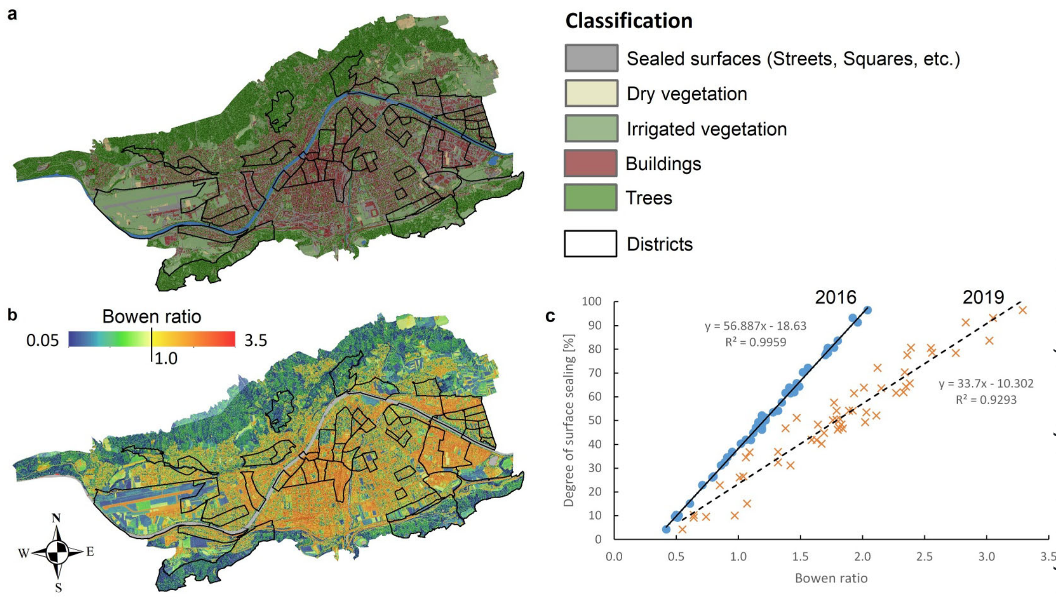

Figure 7. (a) Land cover classification; (b) Bowen ratio across the city of Innsbruck and 53 analyzed districts; (c) Correlation between Bowen ratio and degree of surface sealing for 2016 and 2019.

3.5. Consequences of Maintaining a Prevailing Evaporative Cooling Effect

We analyzed the relationship between the Bowen ratio and degree of surface sealing in 53 randomly selected districts across the city of Innsbruck. The number of districts shows a robust distribution across the Bowen ratio range. Differences in the Bowen ratio due to water-limiting conditions in 2019 were considered, however the degree of surface sealing across the city was assumed to remain unchanged between 2016 and 2019. Using a land cover classification approach (Figure 7a) based on Hiscock et al. (2021), we derived the degree of surface sealing within districts by separating impervious surfaces from vegetated surfaces. Using Equation 4, we derived mean Bowen ratio (Figure 7b) for each district and year. Finally, we plotted the mean values of both variables for each district and year (Figure 7c—blue dots represent conditions in 2016; orange crosses represent conditions in 2019) and found a strong linear relationship ($R^2 = 0.99$ for 2016 and $R^2 = 0.92$ for 2019) between the Bowen ratio and the degree of surface sealing. Finding a strong relationship between the Bowen ratio and the degree of surface sealing is not surprising, given the extensive research on this topic. Earlier studies, such as Oke (1982), have documented the impact of urbanization and surface sealing on the energy balance, showing increased Bowen ratios due to reduced latent heat flux. More recent research, including (Best and Grimmond, 2016), reinforces these findings by demonstrating how increased surface sealing in urban areas continues to elevate the Bowen ratio, thereby contributing to the urban heat island effect.

We combined the linear relationship between the Bowen ratio and the degree of surface sealing with the Bowen ratio-based threshold to describe the surface induced cooling (CE) and warming effect (WE). To achieve a Bowen ratio below 0.52, maintaining a prevailing evaporative cooling effect (CE > WE) and, thus, enhancing micro-climatic conditions, the degree of surface sealing must not exceed 11% within a specified area under normal—wet (2016) conditions (see Figure 8.). Such a low degree of surface sealing is unlikely to be achieved in cities worldwide within short time frames. Innsbruck shows a mean Bowen ratio of 0.95 (2016) and a degree of surface sealing of 35.41%, including the surrounding forests visible in Figures 7a and 7b. This exceeds the targeted 11% to maintain balance between CE and WE by a factor of 3. However, prototypes of specific areas in a city with the potential to achieve such a low degree of surface sealing, conceptually illustrated in Figure 8, can already be found in the concept of superblocks (Eggimann, 2022; Mueller et al., 2020). By reclaiming space from motorized transport (Mueller et al., 2020), the Barcelona superblock promotes a healthier, alternative form of urban design, and is suitable for over 40% of cities' street networks, including irregular street layouts (Eggimann, 2022). A degree of surface sealing below 11% and, thus a Bowen ratio below 0.52, is theoretically achievable, assuming

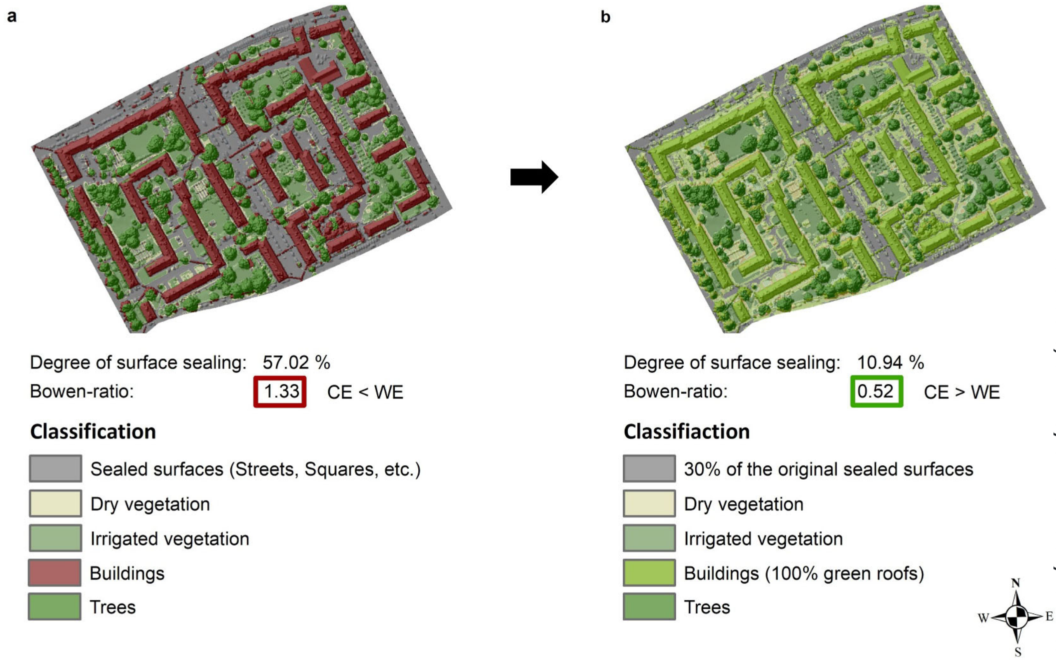

Figure 8. Classification of an area in Innsbruck, the degree of surface sealing and the Bowen ratio-based threshold indicating the surface induced cooling (CE) and warming effect (WE) for (a) the current situation and (b) a potential design with a degree of surface sealing <11%.

unrestricted water supply. Using the concept of Barcelona superblocks, the included surfaces primarily contribute to a cooling effect and thus enhance microclimatic conditions along with many other multiple benefits.

However, as our results for the Innsbruck case study show, urban greening alone is not sufficient to cope with the future consequences posed by climate change. Comparing differences in Bowen ratio between 2016 and 2019 (Figure 7c) emphasizes the necessity of an unrestricted water supply, as no values can be found below a Bowen ratio of 0.52 in the 2019 data set. To maintain vegetation health and an evapotranspiration-driven cooling effect during droughts, sufficient water must be available for green infrastructure to cover such hypothetical superblocks. Even with current interventions such as the Sponge City concept (Nguyen et al., 2019) to increase water infiltration and storage capabilities, the water holding capacities of these interventions are limited, eventually running dry during prolonged dry periods.

3.6. Beyond Current Climate Change Interventions

The combination of increasing temperatures and land aridity and the frequency and intensity of extreme heat events deteriorates diurnal and nocturnal intraurban heat, as well as urban vegetation health, diminishes the evaporative cooling effect, and eventually leads to the degradation of urban ecosystems. If growing cities maintain an urbanization-driven surface sealing, the consequences will increase the number of urban residents exposed to augmented heat stress and water scarcity, mainly affecting socially disadvantaged and vulnerable groups (Benz and Burney, 2021; Hsu et al., 2021) and, thus, reinforcing inequalities worldwide (Alizadeh et al., 2022). Our findings suggest that green infrastructure interventions to reduce urban heat will not be able to cope with future consequences by means of regional water scarcity, if not irrigated extensively. The amount of water needed to maintain vegetation health for a city with a degree of surface sealing below 11%, conceptually illustrated in Figure 9 for the city of Innsbruck, can be stated immense and can hardly be made available naturally in a sustainable way for the majority of cities in the world.

Innsbruck, located in the European Alps, benefits from relatively abundant water resources compared to other regions facing growing water scarcity. Nevertheless, climate change is altering hydrological dynamics across Central Europe, even impacting traditionally water-rich alpine areas (Rakovec et al., 2022; Teuling, 2018). Increased frequency and severity of droughts are stressing regional water supplies, and hydrological regimes are

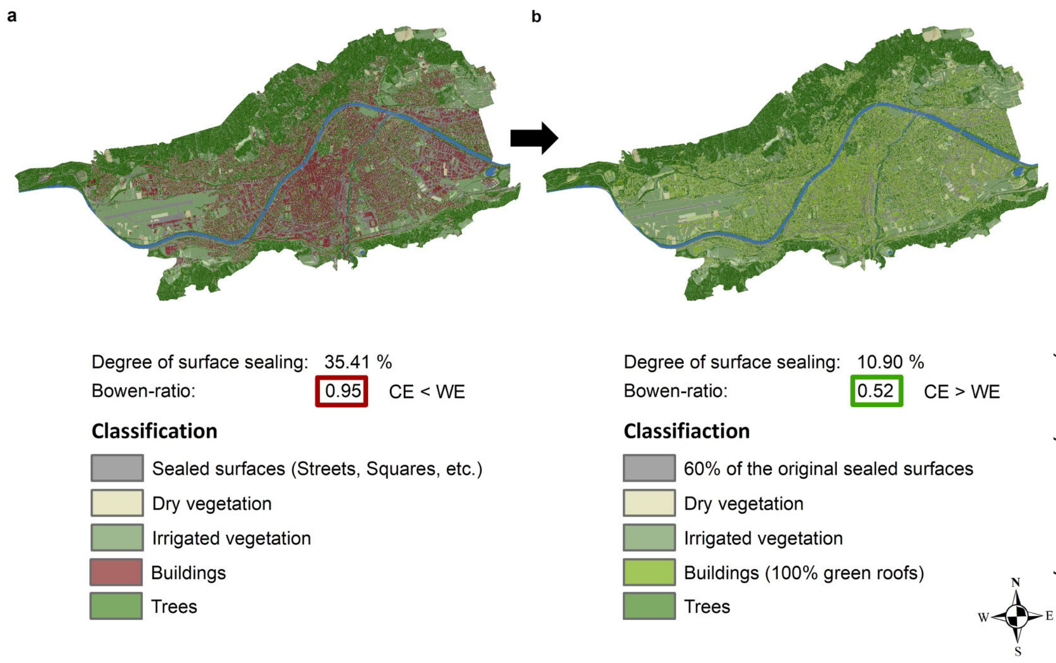

Figure 9. Classification of the city of Innsbruck, the degree of surface sealing and the Bowen ratio-based threshold indicating the surface induced cooling (CE) and warming effect (WE) for (a) the current situation and (b) a potential design with a degree of surface sealing <11%.

shifting due to changes in snow and ice melt patterns (Beniston et al., 2018). These changes disrupt seasonal water storage and reduce runoff and streamflow, enhanced by rising evapotranspiration over land (Mastrotheodoros et al., 2020). Such impacts can be especially severe during dry summer months, straining water availability in both the Alps and downstream lowlands. The European Alps, often termed the "Water Towers of Europe," (Viviroli et al., 2007) play a crucial role in supplying freshwater to surrounding regions. For cities such as Innsbruck, aligning with the United Nations 2030 Agenda for Sustainable Development is essential to secure local water resources and contribute to sustainable urban water management. This approach not only protects local water security, but also supports freshwater availability for downstream lowland regions. Although Innsbruck currently has an adequate water supply, adopting resilient water management practices will help mitigate climate-related risks, ensure long-term water security, and support broader environmental and social stability both at the local scale and beyond.

To reduce pressure on local water resources and prevent an increase in global water challenges (Greve et al., 2018), as well as to secure water demand in agricultural food production, with current water storage solutions (i.e., dam resevoirs) not meeting requirements (Schmitt et al., 2022), innovative solutions are necessary to fully leverage sustainable water resources. Furthermore, in supporting these actions, more resilience-oriented legislative policies are required (Krueger et al., 2019), such as the ABC (Active, Beautiful, Clean) Water Program (ABC guide available under: https://www.pub.gov.sg/abcwaters/designguidelines) in Singapore (Liao, 2019), to for example, overcome land scarcity, especially in highly dense cities, and avoid the collapse of urban water systems.

Especially in mid-latitude cities, urban planning must account for a comprehensive urban water management scheme to connect periods of water surplus and water deficit. Harvesting rainwater and avoiding extraction of groundwater for the irrigation of urban green spaces during the photosynthetic season is essential. With an increase of 1.5°C in global warming, Europe will face cross-sectoral climate impacts (Jacob et al., 2018) and local changes in hydrological processes (Donnelly et al., 2017). In many regions of the world, including Europe and the Southwest of the United States of America, water scarcity is already a present threat, increasing the vulnerability (Büntgen et al., 2021; Mastrotheodoros et al., 2020; Williams et al., 2022). Therefore, augmenting the resilience of cities must involve restoring both natural surface energy and water balance. As such, innovative, certainly also technical, solutions such as recycling water from wastewater treatment plants for green space irrigation (e.g., *third* *pipe water recycling* in Australia (Radcliffe and Page, 2020)) are unavoidable if we are to increase water holding capacities and secure a sustainable means to ensure water availability for successful urban heat mitigation (Livesley et al., 2021) under future climate trajectories. In this regard, recycling rain and greywater has already been shown to potentially reduce potable water demand by 60% when extensively implemented (Zeisl et al., 2018) and can lead to other potential benefits for example, flood reduction (Jamali et al., 2020).

Adequate strategies and interventions in this regard would simultaneously contribute to the achievement of several Sustainable Development Goals (SDGs), promoting well-being, making cities and communities sustainable and resilient, ensuring sustainable consumption, and taking action to cope with the impacts of climate change (UN, 2022). Concurrent drought and extreme heat currently challenge urban planning to its limits in terms of mitigating heat stress and maintaining water availability during extreme events, and thus, call for innovative solutions beyond current climate change interventions. Although this study focuses on the alpine city of Innsbruck, Austria, its findings and insights have broad relevance for cities worldwide. As urban areas across the globe face increasing climate extremes, the impacts on green infrastructure, urban water availability, and human heat stress are becoming more pressing. Our study highlights the critical importance of sustainable water management (SDG 6: Clean Water and Sanitation) and resilient urban infrastructure (SDG 11: Sustainable Cities and Communities) to adapt to these challenges. Unless extensively irrigated, the diminishing cooling effect of green spaces under water-limiting conditions puts additional pressure on local and regional water resources, underscoring the need for innovative approaches to urban water management. To effectively and sustainably maintain green spaces, cities need to integrate practices, such as recycling and reclaiming water from wastewater treatment plants, a measure that also supports SDG 12 (Responsible Consumption and Production). Furthermore, as climate extremes disproportionately impact vulnerable and socially disadvantaged groups, our research emphasizes the importance of urban planning that reduces inequalities in exposure to heat stress and water scarcity, contributing to SDG 10 (Reduced Inequalities). By adopting resilient water management and sustainable green infrastructure practices, cities can help secure long-term water resources, mitigate urban heat, and enhance livability in line with SDG 13 (Climate Action). While Innsbruck currently has relatively abundant water resources, climate-induced changes in hydrological regimes are increasingly stressing, even in traditionally water-rich regions. Therefore, our study provides essential guidance for cities worldwide to integrate resilient water and green infrastructure strategies, not only to support local water security, but also to contribute to broader regional stability, in line with the United Nations' goals for a sustainable, equitable and climate-resilient future.

4. Limitations

To date, the integrated CFD-GIS modeling approach and, hence UTCI calculations are limited to a spatial extent due to the computational time of the CFD simulations. Therefore, UTCI calculations and analyses of the effects of concurrent drought and excessive heat events on human thermal comfort cannot be conducted on a citywide scale. With the Bowen ratio-based threshold, introduced by Back et al. (2024), however, we are able to analyze land-atmosphere interactions, as well as heat transfer between the surface and the atmosphere, and thus locate hotspots across the city. These hotspots typically represent an area corresponding to the spatial extent of possible CFD simulations, without the drawback of computational time. However, the use of NDVI to calculate the Bowen ratio-based threshold to separate the surface induced cooling effect from the warming effect has a drawback in that it is currently only designed for land areas and, therefore, cannot calculate open water areas, including rivers, lakes, and ponds of detectable size. It is also currently not possible to distinguish between wet and dry bare ground. As a result, the Bowen ratio-based approach neglects the potential daytime cooling effect of wet bare ground and only considers evaporative cooling from vegetated areas. The latter, and its interaction with concurrent drought and excessive heat, was the focus of this study. However, the cooling effect of urban water bodies such as rivers can be significant, providing cool retreats, especially on hot summer days (Zhou et al., 2024), and must be considered particularly in urban planning and heat communication strategies.

The underlying CIR image data sets represent two particular points in time in late August 2016 and 2019. Therefore, neither diurnal nor seasonal variations were depicted in this study, nor were specific field measurements that could contribute to the significance of our results and validate the outcomes at the same time. However, the integrated CFD-GIS modeling approach and underlying equations presented as well as the Bowen ratio-based thresholds, describing the surface induced cooling and warming effect on climatic conditions in the urban canopy layer used in this study, have been extensively presented by Back et al. (2023, 2024). This modeling approach includes commonly used equations, vital environmental factors, and well-established physical relations to

10.1029/2024EF005208

accurately represent land-atmosphere processes as well as changes in the vegetation water content and potential evapotranspiration, and their effects on urban micro- and bioclimatic conditions. Further studies at the urban microscale, including measurement campaigns on intraurban climatic conditions that could be used for validation purposes, should be envisaged to close data gaps and provide more in-depth knowledge.

Our study was based on a specific case study in the European Alps. However, our results are also applicable to other cities in different geographical and climatic regions, maintaining the varying climatic conditions and impacts of climate change worldwide. Despite the effects of climate change, changing intraurban meteorological conditions, such as air temperature, wind speed, air humidity, or global radiation, on a daily to seasonal basis, can significantly influence the UTCI impact results shown in this study. Additionally, warmer temperatures, extreme heat, and increased CO_2 levels affect soil and plant-atmosphere interactions and, thus, alter evapotranspiration rates (Allen Jr, 2000; Ben Hamouda et al., 2021). However, our study focused on the effects of concurrent drought and excessive heat on evaporative cooling potential and bioclimatic conditions in cities. Using Innsbruck as an example, we demonstrated that dry vegetation due to a lack of water availability can exacerbate urban overheating by increasing sensible and substrate heat fluxes while simultaneously decreasing the evaporative cooling potential. This phenomenon is particularly relevant for cities at mid-altitudes with pronounced seasonal changes and will become more relevant as climate change increases the frequency and intensity of dry periods. We also emphasize that this phenomenon is not only relevant for many other cities but also for agricultural areas.

5. Conclusions

We demonstrated the effects of the 2019 European summer drought on land-atmosphere interactions, evaporative cooling potential, and human thermal comfort in Innsbruck, Austria, at an intraurban microscale (0.2 m). Using Normalized Difference Vegetation Index (NDVI)-based data sets from August 2016 and 2019, we compared conditions prior to the recorded NDVI image from 2016 (normal—wet) to 2019 (dry) in terms of water availability and analyzed the effects of water scarcity on urban systems. Additionally, we accounted for the global warming-induced increase in daily maximum temperatures of extreme heat days for Innsbruck derived from regional climate simulations conducted in the EURO-CORDEX (Coordinated Regional Downscaling Experiment) initiative and the ReKLiEs (Regional Climate change Ensemble simulations for Germany) project and elaborated on the impacts of concurrent drought and extreme heat on human thermal comfort by means of changes in the Universal Thermal Climate Index (UTCI). Key findings include:

- Using data from regional climate simulations in an urban modeling approach operating at an intraurban microscale is possible and allows to incorporate regional scale climate-driven impacts into intraurban climate modeling.
- Until the end of the century, daily maximum temperature of extreme heat days are projected to increase by 1.0 K in RCP2.6 simulations (mitigation scenario) and by 3.9 K in RCP8.5 simulations (business-as-usual scenario) for the Alpine city of Innsbruck.
- Proportion of areas with Bowen ratios above 2.0, implying a higher proportion of substrate heat fluxes and leading to augmented nocturnal heat transfer from the surface to the atmosphere, increased from 4.3% in 2016 to 21.8% in 2019 within the study area.
- Most vegetated surfaces moved from a wet soil moisture regime and an energy limited evaporative-driven cooling effect (Bowen ratio between 0 and 0.52) to a transitional soil moisture regime and a soil moisture-water limited evaporative-driven cooling effect (Bowen ratio between 0.52 and 1.0), which led to reduced potential evapotranspiration under the conducted simulations.
- Maintaining a prevailing evaporative cooling effect (mean Bowen ratio <0.52) requires a degree of surface sealing <11% and unrestricted water supply.

The complex relationship between surface energy and water fluxes, water availability, vegetation health (including photosynthetic activity and evapotranspiration-driven cooling effect), and outdoor human thermal comfort highlights the connectivity between environmental and human crises in a warming world. Global warming, the intensifying global water cycle and urbanization-driven surface sealing are the main drivers. To reduce health risks and heat-related mortality among urban dwellers and to preserve groundwater availability for future generations, novel comprehensive strategies beyond current climate change interventions are needed to support urban planning. These include combined rain- and greywater recycling and the reclamation of water from the wastewater treatment plant for sustainable irrigation of urban green spaces. Increasing our cities' resilience requires integrated and innovative urban water management that provides sufficient water availability to avoid degradation of ecological systems during prolonged droughts and maintain the evapotranspiration-driven cooling effect during excessive heat events.

Conflict of Interest

The authors declare no conflicts of interest relevant to this study.

Data Availability Statement

The digital elevation model (DEM), the color-infrared (CIR)-image raster, and the building vector layer, used as input data sets in the integrated CFD-GIS modelling approach calculating specific parameters, were provided by the local government “Land Tirol” and are available on request at geoinformation@tirol.gv.at, with further information at https://www.tirol.gv.at/sicherheit/geoinformation/geodaten-tiris/. We used the commercial software packages ESRI ArcMap v10.8.1 (ESRI, 2019) and Ansys® Fluent, Release 2020 R1 (Ansys, 2020) to conduct our analyses and evaluate the simulation results.

Acknowledgments
This work is funded by the Austrian Climate and Energy Fund in the project BlueGreenCities (Project No. KR21KB0K00001), funding period: October 2022 until September 2025 and by the Innsbrucker Kommunalbetriebe (IKB) in the project OptiClim, funding period: June 2022 until Mai 2023. We acknowledge the World Climate Research Programme's Working Group on Regional Climate, and the Working Group on Coupled Modelling, former coordinating body of CORDEX and responsible panel for CMIP5. We also thank the climate modelling groups (listed in Table 1 of this paper) for producing and making available their model output. We also acknowledge the Earth System Grid Federation infrastructure an international effort led by the U.S. Department of Energy's Program for Climate Model Diagnosis and Intercomparison, the European Network for Earth System Modelling and other partners in the Global Organisation for Earth System Science Portals (GO-ESSP). Open access funding provided by Universitat Innsbruck/KEMÖ.

References

Alizadeh, M. R., Abatzoglou, J. T., Adamowski, J. F., Prestemon, J. P., Chittoori, B., Akbari Asanjan, A., & Sadegh, M. (2022). Increasing heat stress inequality in a warming climate. *Earth's Future*, *10*(2), e2021EF002488. https://doi.org/10.1029/2021ef002488

Allen, J. R. L. H. (2000). Evapotranspiration responses of plants and crops to carbon dioxide and temperature. *Journal of Crop Production*, *2*, 37–70. https://doi.org/10.1300/j144v02n02_02

Anderegg, W. R. L., Trugman, A. T., Bowling, D. R., Salvucci, G., & Tuttle, S. E. (2019). Plant functional traits and climate influence drought intensification and land–atmosphere feedbacks. *Proceedings of the National Academy of Sciences*, *116*(28), 14071–14076. https://doi.org/10.1073/pnas.1904747116

ANSYS. (2020). Ansys fluent, release 2020 R1 [Software]. https://www.ansys.com/

Arnbjerg-Nielsen, K., Willems, P., Olsson, J., Beecham, S., Pathirana, A., Bülow Gregersen, I., et al. (2013). Impacts of climate change on rainfall extremes and urban drainage systems: A review. *Water Science and Technology*, *68*(1), 16–28. https://doi.org/10.2166/wst.2013.251

Asseng, S., Spänkuch, D., Hernandez-Ochoa, I. M., & Laporta, J. (2021). The upper temperature thresholds of life. *The Lancet Planetary Health*, *5*(6), e378–e385. https://doi.org/10.1016/s2542-5196(21)00079-6

Back, Y., Bach, P. M., Jasper-Tönnies, A., Rauch, W., & Kleidorfer, M. (2021). A rapid fine-scale approach to modelling urban bioclimatic conditions. *Science of the Total Environment*, *756*, 143732. https://doi.org/10.1016/j.scitotenv.2020.143732

Back, Y., Bach, P. M., Santamouris, M., Rauch, W., & Kleidorfer, M. (2024). Role of surface energy fluxes in urban overheating under buoyancy-driven atmospheric conditions. *Journal of Geophysical Research: Atmospheres*, *129*(13), e2023JD039723. https://doi.org/10.1029/2023jd039723

Back, Y., Kumar, P., Bach, P. M., Rauch, W., & Kleidorfer, M. (2023). Integrating CFD-GIS modelling to refine urban heat and thermal comfort assessment. *Science of the Total Environment*, *858*, 159729. https://doi.org/10.1016/j.scitotenv.2022.159729

Baldwin, J. W., Dessy, J. B., Vecchi, G. A., & Oppenheimer, M. (2019). Temporally compound heat wave events and global warming: An emerging hazard. *Earth's Future*, *7*(4), 411–427. https://doi.org/10.1029/2018ef000989

Bastin, J. F., Clark, E., Elliott, T., Hart, S., Van Den Hoogen, J., Hordijki, I., et al. (2019). Understanding climate change from a global analysis of city analogues. *PLoS One*, *14*(7), e0217592. https://doi.org/10.1371/journal.pone.0217592

Bélair, S., Leroyer, S., Seino, N., Spacek, L., Souvanlasy, V., & Paquin-Ricard, D. (2018). Role and impact of the urban environment in a numerical forecast of an intense summertime precipitation event over Tokyo. *Journal of the Meteorological Society of Japan. Ser. II*, *96A*(0), 77–94. https://doi.org/10.2151/jmsj.2018-011

Ben Hamouda, G., Tomozeiu, R., Pavan, V., Antolini, G., Snyder, R. L., & Ventura, F. (2021). Impacts of climate change and rising atmospheric CO_2 on future projected reference evapotranspiration in Emilia-Romagna (Italy). *Theoretical and Applied Climatology*, *146*(1–2), 801–820. https://doi.org/10.1007/s00704-021-03745-3

Beniston, M., Farinotti, D., Stoffel, M., Andreassen, L. M., Coppola, E., Eckert, N., et al. (2018). The European mountain cryosphere: A review of its current state, trends, and future challenges. *The Cryosphere*, *12*(2), 759–794. https://doi.org/10.5194/tc-12-759-2018

Benz, S. A., & Burney, J. A. (2021). Widespread race and class disparities in surface urban heat extremes across the United States. *Earth's Future*, *9*(7), e2021EF002016. https://doi.org/10.1029/2021ef002016

Berg, A., Findell, K., Lintner, B., Giannini, A., Seneviratne, S. I., Van Den Hurk, B., et al. (2016). Land-atmosphere feedbacks amplify aridity increase over land under global warming. *Nature Climate Change*, *6*(9), 869–874. https://doi.org/10.1038/nclimate3029

Best, M. J., & Grimmond, C. S. B. (2016). Modeling the partitioning of Turbulent fluxes at urban sites with varying vegetation cover. *Journal of Hydrometeorology*, *17*(10), 2537–2553. https://doi.org/10.1175/jhm-d-15-0126.1

Blauhut, V., Stoelzle, M., Ahopelto, L., Brunner, M. I., Teutschbein, C., Wendt, D. E., et al. (2022). Lessons from the 2018–2019 European droughts: A collective need for unifying drought risk management. *Natural Hazards and Earth System Sciences*, *22*(6), 2201–2217. https://doi.org/10.5194/nhess-22-2201-2022

Bröde, P., Jendritzky, G., Fiala, D., & Havenith, G. (2010). The universal thermal climate index UTCI in operational use. In *Windsor Conference, UK* (pp. 9–11).

Büntgen, U., Urban, O., Krusic, P. J., Rybníček, M., Kolář, T., Kyncl, T., et al. (2021). Recent European drought extremes beyond Common Era background variability. *Nature Geoscience*, *14*(4), 190–196. https://doi.org/10.1038/s41561-021-00698-0

Chan, S. K., Bindlish, R., Hunt, J. R. E. R., Jackson, T., & Kimball, J. (2013). *Soil Moisture Active Passive (SMAP) ancillary data report—vegetation water content*. NASA Jet Propulsion Laboratory. Retrieved from https://smap.jpl.nasa.gov/system/internal_resources/details/original/289_047_veg_water.pdf

10.1029/2024EF005208

Chocat, B., Krebs, P., Marsalek, J., Rauch, W., & Schilling, W. (2001). Urban drainage redefined: From stormwater removal to integrated management. *Water Science and Technology*, *43*(5), 61–68. https://doi.org/10.2166/wst.2001.0251

Cook, B. I., Mankin, J. S., Marvel, K., Williams, A. P., Smerdon, J. E., & Anchukaitis, K. J. (2020). Twenty-first century drought projections in the CMIP6 forcing scenarios. *Earth's Future*, *8*(6), e2019EF001461. https://doi.org/10.1029/2019ef001461

Daniel, M., Lemonsu, A., Déqué, M., Somot, S., Alias, A., & Masson, V. (2019). Benefits of explicit urban parameterization in regional climate modeling to study climate and city interactions. *Climate Dynamics*, *52*(5–6), 2745–2764. https://doi.org/10.1007/s00382-018-4289-x

Dirmeyer, P. A., Cash, B. A., Kinter, J. L., Stan, C., Jung, T., Marx, L., et al. (2012). Evidence for enhanced land–atmosphere feedback in a warming climate. *Journal of Hydrometeorology*, *13*(3), 981–995. https://doi.org/10.1175/jhm-d-11-0104.1

Doan, Q.-V., Chen, F., Kusaka, H., Dipankar, A., Khan, A., Hamdi, R., et al. (2022). Increased risk of extreme precipitation over an urban agglomeration with future global warming. *Earth's Future*, *10*(6), e2021EF002563. https://doi.org/10.1029/2021ef002563

Donnelly, C., Greuell, W., Andersson, J., Gerten, D., Pisacane, G., Roudier, P., & Ludwig, F. (2017). Impacts of climate change on European hydrology at 1.5, 2 and 3 degrees mean global warming above preindustrial level. *Climatic Change*, *143*(1–2), 13–26. https://doi.org/10.1007/s10584-017-1971-7

Eggimann, S. (2022). The potential of implementing superblocks for multifunctional street use in cities. *Nature Sustainability*, *5*, 406–414. https://doi.org/10.1038/s41893-022-00855-2

ESRI. (2019). ArcGIS desktop: Release 10 [Software]. *Redlands, California*. Retrieved from https://www.esri.com/en-us/arcgis/products/arcgis-desktop/resources

Fischer, E. M., Sippel, S., & Knutti, R. (2021). Increasing probability of record-shattering climate extremes. *Nature Climate Change*, *11*(8), 689–695. https://doi.org/10.1038/s41558-021-01092-9

Gent, P. R., Danabasoglu, G., Donner, L. J., Holland, M. M., Hunke, E. C., Jayne, S. R., et al. (2011). The community climate system model version 4. *Journal of Climate*, *24*(19), 4973–4991. https://doi.org/10.1175/2011jcli4083.1

Geosphere Austria. (2024). Klimamonitoring. [Online]. www.zamg.ac.at/cms/de/klima/klima-aktuell/klimamonitoring. Accessed 25.03 2024.

Gerken, T., Ruddell, B. L., Yu, R., Stoy, P. C., & Drewry, D. T. (2019). Robust observations of land-to-atmosphere feedbacks using the information flows of FLUXNET. *npj Climate and Atmospheric Science*, *2*(1), 37. https://doi.org/10.1038/s41612-019-0094-4

Giorgi, F., Jones, C., & Asrar, G. R. (2009). Addressing climate information needs at the regional level: The CORDEX framework. *World Meteorological Organization (WMO) Bulletin*, *58*(3), 175.

Gobiet, A., Kotlarski, S., Beniston, M., Heinrich, G., Rajczak, J., & Stoffel, M. (2014). 21st century climate change in the European Alps—A review. *Science of the Total Environment*, *493*, 1138–1151. https://doi.org/10.1016/j.scitotenv.2013.07.050

Greve, P., Kahil, T., Mochizuki, J., Schinko, T., Satoh, Y., Burek, P., et al. (2018). Global assessment of water challenges under uncertainty in water scarcity projections. *Nature Sustainability*, *1*(9), 486–494. https://doi.org/10.1038/s41893-018-0134-9

Held, I. M., & Soden, B. J. (2006). Robust responses of the hydrological cycle to global warming. *Journal of Climate*, *19*(21), 5686–5699. https://doi.org/10.1175/jcli3990.1

Hirsch, A. L., Pitman, A. J., & Kala, J. (2014). The role of land cover change in modulating the soil moisture-temperature land-atmosphere coupling strength over Australia. *Geophysical Research Letters*, *41*(16), 5883–5890. https://doi.org/10.1002/2014gl061179

Hiscock, O. H., Back, Y., Kleidorfer, M., & Urich, C. (2021). A GIS-based land cover classification approach suitable for fine-scale urban water management. *Water Resources Management*, *35*(4), 1339–1352. https://doi.org/10.1007/s11269-021-02790-x

Hoffmann, P., Menz, C., & Spekat, A. (2018). Bias adjustment for threshold-based climate indicators. *Advances in Science and Research*, *15*, 107–116. https://doi.org/10.5194/asr-15-107-2018

Hsu, A., Sheriff, G., Chakraborty, T., & Manya, D. (2021). Disproportionate exposure to urban heat island intensity across major US cities. *Nature Communications*, *12*(1), 2721. https://doi.org/10.1038/s41467-021-22799-5

Huntington, T. G. (2006). Evidence for intensification of the global water cycle: Review and synthesis. *Journal of Hydrology*, *319*(1–4), 83–95. https://doi.org/10.1016/j.jhydrol.2005.07.003

Jach, L., Schwitalla, T., Branch, O., Warrach-Sagi, K., & Wulfmeyer, V. (2022). Sensitivity of land–atmosphere coupling strength to changing atmospheric temperature and moisture over Europe. *Earth Syst. Dynam.*, *13*(1), 109–132. https://doi.org/10.5194/esd-13-109-2022

Jacob, D., Kotova, L., Teichmann, C., Sobolowski, S. P., Vautard, R., Donnelly, C., et al. (2018). Climate impacts in Europe under +1.5°C global warming. *Earth's Future*, *6*(2), 264–285. https://doi.org/10.1002/2017ef000710

Jacob, D., Petersen, J., Eggert, B., Alias, A., Christensen, O. B., Bouwer, L. M., et al. (2014). EURO-CORDEX: New high-resolution climate change projections for European impact research. *Regional Environmental Change*, *14*(2), 563–578. https://doi.org/10.1007/s10113-013-0499-2

Jaeger, E. B., & Seneviratne, S. I. (2011). Impact of soil moisture–atmosphere coupling on European climate extremes and trends in a regional climate model. *Climate Dynamics*, *36*(9–10), 1919–1939. https://doi.org/10.1007/s00382-010-0780-8

Jamali, B., Bach, P. M., & Deletic, A. (2020). Rainwater harvesting for urban flood management – An integrated modelling framework. *Water Research*, *171*, 115372. https://doi.org/10.1016/j.watres.2019.115372

Jeong, D. I., Sushama, L., Diro, G. T., Khaliq, M. N., Beltrami, H., & Caya, D. (2016). Projected changes to high temperature events for Canada based on a regional climate model ensemble. *Climate Dynamics*, *46*(9–10), 3163–3180. https://doi.org/10.1007/s00382-015-2759-y

Kotlarski, S., Paul, F., & Jacob, D. (2010). Forcing a distributed glacier mass balance model with the regional climate model REMO. Part I: Climate model evaluation. *Journal of Climate*, *23*(6), 1589–1606. https://doi.org/10.1175/2009jcli2711.1

Krueger, E. H., Borchardt, D., Jawitz, J. W., Klammler, H., Yang, S., Zischg, J., & Rao, P. S. C. (2019). Resilience dynamics of urban water supply security and potential of tipping points. *Earth's Future*, *7*(10), 1167–1191. https://doi.org/10.1029/2019ef001306

Kustas, W. P., & Daughtry, C. S. T. (1990). Estimation of the soil heat flux/net radiation ratio from spectral data. *Agricultural and Forest Meteorology*, *49*(3), 205–223. https://doi.org/10.1016/0168-1923(90)90033-3

Lafortezza, R., Chen, J., Van Den Bosch, C. K., & Randrup, T. B. (2018). Nature-based solutions for resilient landscapes and cities. *Environmental Research*, *165*, 431–441. https://doi.org/10.1016/j.envres.2017.11.038

Lai, D., Liu, W., Gan, T., Liu, K., & Chen, Q. (2019). A review of mitigating strategies to improve the thermal environment and thermal comfort in urban outdoor spaces. *Science of the Total Environment. Elsevier B.V*, *661*, 337–353. https://doi.org/10.1016/j.scitotenv.2019.01.062

Lang, D., Zheng, J., Shi, J., Liao, F., Ma, X., Wang, W., et al. (2017). A comparative study of potential evapotranspiration estimation by eight methods with FAO Penman–Monteith method in southwestern China. *Water (Switzerland)*, *9*(10), 734. https://doi.org/10.3390/w9100734

Langendijk, G. S., Rechid, D., & Jacob, D. (2019). Urban areas and urban–Rural contrasts under climate change: What does the EURO-CORDEX ensemble tell Us? Investigating near surface humidity in Berlin and its surroundings. *Atmosphere*, *10*(12), 730. https://doi.org/10.3390/atmos10120730

Lian, X., Piao, S., Li Laurent, Z. X., Li, Y., Huntingford, C., Ciais, P., et al. (2020). Summer soil drying exacerbated by earlier spring greening of northern vegetation. *Science Advances*, *6*(1), eaax0255. https://doi.org/10.1126/sciadv.aax0255

Liao, K.-H. (2019). The socio-ecological practice of building blue-green infrastructure in high-density cities: What does the ABC waters Program in Singapore tell us? *Socio-Ecological Practice Research*, *1*, 67–81. https://doi.org/10.1007/s42532-019-00009-3

Li, D., Liao, W., Rigden, A. J., Liu, X., Wang, D., Malyshev, S., & Shevliakova, E. (2019). Urban heat island: Aerodynamics or imperviousness? *Science*, *5*(4). https://doi.org/10.1126/sciadv.aau4299

Livesley, S. J., Marchionni, V., Cheung, P. K., Daly, E., & Pataki, D. E. (2021). Water smart cities increase irrigation to provide cool refuge in a climate crisis. *Earth's Future*, *9*(1), e2020EF001806. https://doi.org/10.1029/2020ef001806

Lorenz, R., Argüeso, D., Donat, M. G., Pitman, A. J., Van Den Hurk, B., Berg, A., et al. (2016). Influence of land-atmosphere feedbacks on temperature and precipitation extremes in the GLACE-CMIP5 ensemble. *Journal of Geophysical Research: Atmospheres*, *121*(2), 607–623. https://doi.org/10.1002/2015jd024053

Maes, M. J. A., Pirani, M., Booth, E. R., Shen, C., Milligan, B., Jones, K. E., & Toledano, M. B. (2021). Benefit of woodland and other natural environments for adolescents' cognition and mental health. *Nature Sustainability*, *4*(10), 851–858. https://doi.org/10.1038/s41893-021-00751-1

Manoli, G., Fatichi, S., Bou-Zeid, E., & Katul, G. G. (2020). Seasonal hysteresis of surface urban heat islands. *PNAS*, *117*(13), 7082–7089. https://doi.org/10.1073/pnas.1917554117

Manoli, G., Fatichi, S., Schläpfer, M., Yu, K., Crowther, T. W., Meili, N., et al. (2019). Magnitude of urban heat islands largely explained by climate and population. *Nature*, *573*(7772), 55–60. https://doi.org/10.1038/s41586-019-1512-9

Mastrotheodoros, T., Pappas, C., Molnar, P., Burlando, P., Manoli, G., Parajka, J., et al. (2020). More green and less blue water in the Alps during warmer summers. *Nature Climate Change*, *10*(2), 155–161. https://doi.org/10.1038/s41558-019-0676-5

Matsler, A. M., Meerow, S., Mell, I. C., & Pavao-Zuckerman, M. A. (2021). A "green" chameleon: Exploring the many disciplinary definitions, goals, and forms of "green infrastructure". *Landscape and Urban Planning*, *214*, 104145. https://doi.org/10.1016/j.landurbplan.2021.104145

Matzarakis, A., Rutz, F., & Mayer, H. (2010). Modelling radiation fluxes in simple and complex environments: Basics of the RayMan model. *International Journal of Biometeorology*, *54*(2), 131–139. https://doi.org/10.1007/s00484-009-0261-0

Mazdiyasni, O., & Aghakouchak, A. (2015). Substantial increase in concurrent droughts and heatwaves in the United States. *Proceedings of the National Academy of Sciences*, *112*(37), 11484–11489. https://doi.org/10.1073/pnas.1422945112

Mccarthy, M. P., Best, M. J., & Betts, R. A. (2010). Climate change in cities due to global warming and urban effects. *Geophysical Research Letters*, *37*(9). https://doi.org/10.1029/2010gl042845

Mcmahon, T. A., Peel, M. C., Lowe, L., Srikanthan, R., & Mcvicar, T. R. (2013). Estimating actual, potential, reference crop and pan evaporation using standard meteorological data: A pragmatic synthesis. *Hydrology and Earth System Sciences*, *17*(4), 1331–1363. https://doi.org/10.5194/hess-17-1331-2013

Meili, N., Manoli, G., Burlando, P., Bou-Zeid, E., Chow, W. T. L., Coutts, A. M., et al. (2020). An urban ecohydrological model to quantify the effect of vegetation on urban climate and hydrology (UT&C v1.0). *Geoscientific Model Development*, *13*, 335–362.

Moss, R. H., Edmonds, J. A., Hibbard, K. A., Manning, M. R., Rose, S. K., Van Vuuren, D. P., et al. (2010). The next generation of scenarios for climate change research and assessment. *Nature*, *463*(7282), 747–756. https://doi.org/10.1038/nature08823

Mueller, N., Rojas-Rueda, D., Khreis, H., Cirach, M., Andrés, D., Ballester, J., et al. (2020). Changing the urban design of cities for health: The superblock model. *Environment International*, *134*, 105132. https://doi.org/10.1016/j.envint.2019.105132

Nazarian, N., Krayenhoff, E. S., Bechtel, B., Hondula, D. M., Paolini, R., Vanos, J., et al. (2022). Integrated assessment of urban overheating impacts on human life. *Earth's Future*, *10*(8), e2022EF002682. https://doi.org/10.1029/2022ef002682

Nesshöver, C., Assmuth, T., Irvine, K. N., Rusch, G. M., Waylen, K. A., Delbaere, B., et al. (2017). The science, policy and practice of nature-based solutions: An interdisciplinary perspective. *Science of the Total Environment. Elsevier B.V.*

Nguyen, T. T., Ngo, H. H., Guo, W., Wang, X. C., Ren, N., Li, G., et al. (2019). Implementation of a specific urban water management—Sponge City. *Science of the Total Environment. Elsevier B.V*, *652*, 147–162. https://doi.org/10.1016/j.scitotenv.2018.10.168

O'Gorman, P. A., & Muller, C. J. (2010). How closely do changes in surface and column water vapor follow Clausius–Clapeyron scaling in climate change simulations? *Environmental Research Letters*, *5*(2), 025207. https://doi.org/10.1088/1748-9326/5/2/025207

Oh, S.-G., & Sushama, L. (2021). Urban-climate interactions during summer over eastern North America. *Climate Dynamics*, *57*(11–12), 3015–3028. https://doi.org/10.1007/s00382-021-05852-3

Oke, T. R. (1982). The energetic basis of the urban heat island. *Quarterly Journal of the Royal Meteorological Society*, *108*(455), 1–24. https://doi.org/10.1002/qj.49710845502

Oleson, K. W., Bonan, G. B., Feddema, J., & Jackson, T. (2011). An examination of urban heat island characteristics in a global climate model. *International Journal of Climatology*, *31*(12), 1848–1865. https://doi.org/10.1002/joc.2201

Oleson, K. W., Bonan, G. B., Feddema, J., Vertenstein, M., & Grimmond, C. S. B. (2008). An urban parameterization for a global climate model. Part I formulation and evaluation for two cities. *Journal of Applied Meteorology and Climatology*, *47*(4), 1038–1060. https://doi.org/10.1175/2007jamc1597.1

Oleson, K. (2012). Contrasts between urban and rural climate in CCSM4 CMIP5 climate change scenarios. *Journal of Climate*, *25*(5), 1390–1412. https://doi.org/10.1175/jcli-d-11-00098.1

Parkinson, S. (2021). Guiding urban water management towards 1.5°C. *npj Clean Water. Nature Research*, *4*(1), 34. https://doi.org/10.1038/s41545-021-00126-1

Parlow, E. (2003). The urban heat budget derived from satellite data. *Geographica Helvetica*, *58*(2), 99–111. https://doi.org/10.5194/gh-58-99-2003

Pendergrass, A. G., & Hartmann, D. L. (2014). The atmospheric energy constraint on global-mean precipitation change. *Journal of Climate*, *27*(2), 757–768. https://doi.org/10.1175/jcli-d-13-00163.1

Peng, S., Piao, S., Ciais, P., Friedlingstein, P., Ottle, C., Bréon, F. M., et al. (2012). Surface urban heat island across 419 global big cities. *Environmental Science and Technology*, *46*(2), 696–703. https://doi.org/10.1021/es2030438

Priestley, C. H. B., & Taylor, R. J. (1972). On the assessment of surface heat flux and evaporation using large-scale parameters. *Monthly Weather Review*, *100*(2), 81–92. https://doi.org/10.1175/1520-0493(1972)100<0081:otaosh>2.3.co;2

Radcliffe, J. C., & Page, D. (2020). Water reuse and recycling in Australia — History, current situation and future perspectives. *Water Cycle*, *1*, 19–40. https://doi.org/10.1016/j.watcyc.2020.05.005

Rakovec, O., Samaniego, L., Hari, V., Markonis, Y., Moravec, V., Thober, S., et al. (2022). The 2018–2020 multi-year drought sets a new benchmark in Europe. *Earth's Future*, *10*(3), e2021EF002394. https://doi.org/10.1029/2021ef002394

Rigo, G. (2006). *Satellite analysis of radiation and heat fluxes during the Basel Urban Boundary Layer Experiment (BUBBLE)* (Doctoral Thesis). University of Basel, Faculty of Science. https://doi.org/10.5451/unibas-004053395

Rigo, G., & Parlow, E. (2007). Modelling the ground heat flux of an urban area using remote sensing data. *Theoretical and Applied Climatology*, *90*(3–4), 185–199. https://doi.org/10.1007/s00704-006-0279-8

Ruangpan, L., Vojinovic, Z., Di Sabatino, S., Leo, L. S., Capobianco, V., Oen, A. M. P., et al. (2020). Nature-based solutions for hydro-meteorological risk reduction: A state-of-the-art review of the research area. *Natural Hazards and Earth System Sciences*, *20*(1), 243–270. https://doi.org/10.5194/nhess-20-243-2020

Santanello, J. A., Dirmeyer, P. A., Ferguson, C. R., Findell, K. L., Tawfik, A. B., Berg, A., et al. (2018). Land–atmosphere interactions: The LoCo perspective. *Bulletin of the American Meteorological Society*, *99*(6), 1253–1272. https://doi.org/10.1175/bams-d-17-0001.1

Scheff, J., & Frierson, D. M. W. (2014). Scaling potential evapotranspiration with greenhouse warming. *Journal of Climate*, *27*(4), 1539–1558. https://doi.org/10.1175/jcli-d-13-00233.1

Schmitt, R. J. P., Rosa, L., & Daily, G. C. (2022). Global expansion of sustainable irrigation limited by water storage. *Proceedings of the National Academy of Sciences*, *119*(47), e2214291119. https://doi.org/10.1073/pnas.2214291119

Schumacher, D. L., Keune, J., Dirmeyer, P., & Miralles, D. G. (2022). Drought self-propagation in drylands due to land–atmosphere feedbacks. *Nature Geoscience*, *15*(4), 262–268. https://doi.org/10.1038/s41561-022-00912-7

Seneviratne, S. I., Corti, T., Davin, E. L., Hirschi, M., Jaeger, E. B., Lehner, I., et al. (2010). Investigating soil moisture-climate interactions in a changing climate: A review. *Earth-Science Reviews*, *99*(3–4), 125–161. https://doi.org/10.1016/j.earscirev.2010.02.004

Seneviratne, S. I., Lüthi, D., Litschi, M., & Schär, C. (2006). Land–atmosphere coupling and climate change in Europe. *Nature*, *443*(7108), 205–209. https://doi.org/10.1038/nature05095

Smiatek, G., Kunstmann, H., & Senatore, A. (2016). EURO-CORDEX regional climate model analysis for the Greater Alpine Region: Performance and expected future change. *Journal of Geophysical Research: Atmospheres*, *121*(13), 7710–7728. https://doi.org/10.1002/2015jd024727

Sousa, P. M., Barriopedro, D., García-Herrera, R., Ordóñez, C., Soares, P. M. M., & Trigo, R. M. (2020). Distinct influences of large-scale circulation and regional feedbacks in two exceptional 2019 European heatwaves. *Communications Earth & Environment*, *1*, 48. https://doi.org/10.1038/s43247-020-00048-9

Taylor, K. E., Stouffer, R. J., & Meehl, G. A. (2012). An overview of CMIP5 and the experiment design. *Bulletin of the American Meteorological Society*, *93*(4), 485–498. https://doi.org/10.1175/bams-d-11-00094.1

Teuling, A. J. (2018). A hot future for European droughts. *Nature Climate Change*, *8*(5), 364–365. https://doi.org/10.1038/s41558-018-0154-5

Tomczyk, A. M., & Owczarek, M. (2020). Occurrence of strong and very strong heat stress in Poland and its circulation conditions. *Theoretical and Applied Climatology*, *139*(3–4), 893–905. https://doi.org/10.1007/s00704-019-02998-3

UN. (2022). *The sustainable development goals report 2022*. United Nations.

Van Vuuren, D. P., Edmonds, J., Kainuma, M., Riahi, K., Thomson, A., Hibbard, K., et al. (2011). The representative concentration pathways: An overview. *Climatic Change*, *109*(1–2), 5–31. https://doi.org/10.1007/s10584-011-0148-z

Vautard, R., Gobiet, A., Jacob, D., Belda, M., Colette, A., Déqué, M., et al. (2013). The simulation of European heat waves from an ensemble of regional climate models within the EURO-CORDEX project. *Climate Dynamics*, *41*(9–10), 2555–2575. https://doi.org/10.1007/s00382-013-1714-z

Viviroli, D., Dürr, H. H., Messerli, B., Meybeck, M., & Weingartner, R. (2007). Mountains of the world, water towers for humanity: Typology, mapping, and global significance. *Water Resources Research*, *43*(7). https://doi.org/10.1029/2006wr005653

Wang, R., Li, L., Gentine, P., Zhang, Y., Chen, J., Chen, X., et al. (2022). Recent increase in the observation-derived land evapotranspiration due to global warming. *Environmental Research Letters*, *17*(2), 024020. https://doi.org/10.1088/1748-9326/ac4291

Williams, A. P., Cook, B. I., & Smerdon, J. E. (2022). Rapid intensification of the emerging southwestern North American megadrought in 2020–2021. *Nature Climate Change*, *12*(3), 232–234. https://doi.org/10.1038/s41558-022-01290-z

Xu, P., Wang, L., Liu, Y., Chen, W., & Huang, P. (2020). The record-breaking heat wave of June 2019 in Central Europe. *Atmospheric Science Letters*, *21*(4), e964. https://doi.org/10.1002/asl.964

Zeisl, P., Mair, M., Kastlunger, U., Bach, P. M., Rauch, W., Sitzenfrei, R., & Kleidorfer, M. (2018). Conceptual urban water balance model for water policy testing: An approach for large scale investigation. *Sustainability*, *10*(3), 716. https://doi.org/10.3390/su10030716

Zhang, Z., Paschalis, A., Mijic, A., Meili, N., Manoli, G., Van Reeuwijk, M., & Fatichi, S. (2022). A mechanistic assessment of urban heat island intensities and drivers across climates. *Urban Climate*, *44*, 101215. https://doi.org/10.1016/j.uclim.2022.101215

Zhao, L., Oleson, K., Bou-Zeid, E., Krayenhoff, E. S., Bray, A., Zhu, Q., et al. (2021). Global multi-model projections of local urban climates. *Nature Climate Change*, *11*(2), 152–157. https://doi.org/10.1038/s41558-020-00958-8

Zhou, D., Xiao, J., Frolking, S., Zhang, L., & Zhou, G. (2022). Urbanization contributes little to global warming but substantially intensifies local and regional land surface warming. *Earth's Future*, *10*(5), e2021EF002401. https://doi.org/10.1029/2021ef002401

Zhou, S., Williams, A. P., Berg, A. M., Cook, B. I., Zhang, Y., Hagemann, S., et al. (2019). Land–atmosphere feedbacks exacerbate concurrent soil drought and atmospheric aridity. *Proceedings of the National Academy of Sciences*, *116*(38), 18848–18853. https://doi.org/10.1073/pnas.1904955116

Zhou, S., & Yu, B. (2024). Physical basis of the potential evapotranspiration and its estimation over land. *Journal of Hydrology*, *641*, 131825. https://doi.org/10.1016/j.jhydrol.2024.131825

Zhou, W., Wu, T., & Tao, X. (2024). Exploring the spatial and seasonal heterogeneity of cooling effect of an urban river on a landscape scale. *Scientific Reports*, *14*(1), 8327. https://doi.org/10.1038/s41598-024-58879-x